Available online at www.sciencedirect.com
ScienceDirect
Publishing Services by Elsevier
International Journal of Naval Architecture and Ocean Engineering xx (2016) 1–22
http://www.journals.elsevier.com/international-journal-of-naval-architecture-and-ocean-engineering/

Simulation of a two-stroke diesel engine for propulsion in waves

Kevin Koosup Yum*, Bhushan Taskar, Eilif Pedersen, Sverre Steen

Department of Marine Technology, Norwegian University of Science and Technology, Trondheim, Norway

Received 1 June 2016; accepted 25 August 2016
Available online ■ ■ ■

Abstract

Propulsion in waves is a complex physical process that involves interactions between a hull, a propeller, a shaft and a prime mover which is often a diesel engine. Among the relevant components, the diesel engine plays an important role in the overall system dynamics. Therefore, using a proper model for the diesel engine is essential to achieve the reasonable accuracy of the transient simulation of the entire system. In this paper, a simulation model of a propulsion system in waves is presented with emphasis on modeling a two-stroke marine diesel engine: the framework for building such a model and its mathematical descriptions. The models are validated against available measurement data, and a sensitivity analysis for the transient performance of the diesel engine is carried out. Finally, the results of the system simulations under various wave conditions are analyzed to understand the physical processes and compare the efficiency for different cases.
Copyright © 2016 Society of Naval Architects of Korea. Production and hosting by Elsevier B.V. This is an open access article under the CC BY-NC-ND license (http://creativecommons.org/licenses/by-nc-nd/4.0/).

Keywords: Two-stroke diesel engine; Propulsion in waves; System simulation

1. Introduction

Ships traveling in waves encounter various challenges. The added resistance due to waves and wind causes the ship speed to drop and lowers its maneuverability. The speed drop will increase the propeller loading and decrease the efficiency, for which the main engine may struggle to produce the required torque. Furthermore, the load torque on the main engine varies periodically due to the variation of the propeller inflow, induced both by wave mechanics and ship motions. In harsher weather, the propeller may even come out of water, which will result in a sudden loss of propeller torque and a rapid increase of the engine shaft speed. This may lead to overspeeding of the main engine, and the speed protection could trip the engine. The effects of waves on the ship's propulsion is a complex phenomenon involving the interactions between environmental loads, the vessel dynamics and the propulsion system response as shown in Fig. 1 Taskar et al. (2016).

The diesel engine provides necessary power to the propulsion system, and it plays a dominant role in the system dynamics. Most marine diesel engines are equipped with turbochargers, and their transient characteristics, so-called "turbo-lag", make them a slower part of the overall system. Therefore, it is crucial to understand the dynamics of the diesel engine system in relation to the overall system response during the design of the system, especially for sizing the main engine.

Energy Efficiency Design Index (EEDI) introduced by the International Maritime Organization (IMO) has provided an important framework for reducing green house gas (GHG) emission from the shipping industry. However, the formulation for EEDI favors reducing the installed power of the main engine, which might tempts the designers to do so without applying innovative designs (Papanikolaou et al., 2014). If so, the vessel may not have the sufficient power to maintain its speed or maneuverability in harsh weather. On the other hand, adding a design margin for possible off-design conditions without a proper analysis may be a costly solution. In this regard, finding the optimal power rating of a propulsion plant has become more important than ever.

* Corresponding author.
E-mail address: kevin.koosup.yum@ntnu.no (K.K. Yum).
Peer review under responsibility of Society of Naval Architects of Korea.

http://dx.doi.org/10.1016/j.ijnaoe.2016.08.004
2092-6782/Copyright © 2016 Society of Naval Architects of Korea. Production and hosting by Elsevier B.V. This is an open access article under the CC BY-NC-ND license (http://creativecommons.org/licenses/by-nc-nd/4.0/).

Please cite this article in press as: Yum, K.K., et al., Simulation of a two-stroke diesel engine for propulsion in waves, International Journal of Naval Architecture and Ocean Engineering (2016), http://dx.doi.org/10.1016/j.ijnaoe.2016.08.004

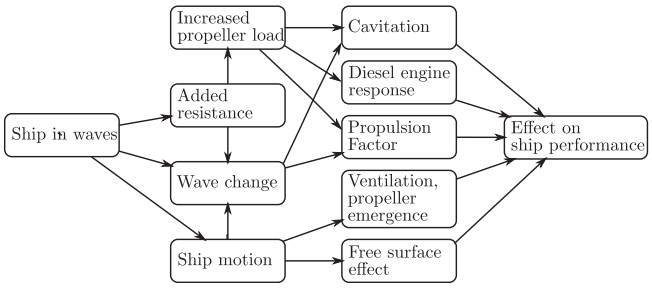

Fig. 1. Effect of waves on the ship propulsion (Taskar et al., 2016).

Using dynamic numerical simulations for a hull-propeller-diesel engine system can be a good tool in the optimization process, saving time and cost of ship designs. A number of system analyses by simulations are found in the literature. The work by Kyrtatos et al. (1999) and Campora and Figari (2005) both utilized a high fidelity model of the diesel engine which simulate physical processes for combustion, heat transfer or a gas exchanging process in a phenomenological way. In these engine models, an engine cycle is simulated at crank angle resolution so that the high frequency torque variation and the efficiency of each engine cycle can be obtained from the physical based models. In the former paper, the propeller torque is given as time-series data from measurements. Therefore, there are limitations to generalize the result of the simulation. In the latter work, simulations were validated to the full-scale measurements during maneuvering operations. In the simulations, a logical telegraph gave identical telegraph commands, which were obtained during the measurement, to the engine governor and the pitch controller of the propeller in order to compare the simulated response of the physical systems to measurements. Still, the effect of the waves is not accounted in the model and could be a potential reason for the gaps between the simulations and the measurements.

A study by el Moctar et al. (2014) provides a unique method coupling Computational Fluid Dynamics (CFD) analysis with a dynamic engine model. In this work, the diesel engine is modeled as a parametric model where only the mechanical dynamics of the system is accounted for. However, the model provides proper boundary conditions for the CFD analysis which simulated the vessel and its propulsion system in the sea trial cases under mild sea conditions. This work shows potential for using the tool for verification of ship designs in the final stage: however, due to the computational intensiveness of CFD calculations, it is difficult to utilize it as a tool for the wider search of design parameters.

Using such high fidelity models is valuable for the analysis of the propulsion system in waves because the systems are often in the off-design conditions where the model parameters from the steady state analysis are not available or applicable. However, the challenge is that the diesel engine itself is a complex system to model and requires extensive parameters and thorough validation of the model. Therefore, a systematic method to build and evaluate such a model is necessary.

In this paper, we try to achieve: i) to provide a systematic procedure of building the dynamic system model for hull-propeller-diesel engine simulations with a particular emphasis on modeling a diesel engine and ii) to provide the insights into the response of the propulsion system in waves by analyzing the result of the numerical simulations. In the first part of the paper, the modeling framework and the modeling process is presented. Then, the descriptions of the physical and mathematical models of the subsystems are given in detail, followed by validation of the individual models. The results of dynamic system simulations are provided for various wave cases with the explanation of relationship between the system response and the physical processes. Finally, the analysis of the system efficiency is presented for the simulation cases, and the influence of transient loads on the diesel engine efficiency is evaluated.

2. Modeling framework

Building a numerical simulation model is an iterative process where a modeler should identify definite goals of the simulation and, thereby, determine the relevant physical models, then find a way to implement them into computerized models. Therefore, it is beneficial to define the modeling framework before starting the process. The modeling framework includes the following:

- definition of the purpose of the simulation,
- selection of the physical processes to be modeled,
- selection of the proper models to describe the physical processes,
- definition of the system variables and system-level interface structure.

2.1. Purpose of the simulation

The purposes of the simulation for the propulsion system in waves are: (1) to simulate the time-domain response of the propulsion system in waves, (2) to simulate the propeller-diesel engine interaction, in particular, in terms of shaft speed and efficiency and (3) to observe the engine system behavior in such conditions. In order to achieve the goals, the engine system model should be able to provide dynamic shaft torque and predict the cycle efficiency of the engine under transient load conditions. In addition, the simulation speed should be at least in the same order of magnitude as real-time.

2.2. Scope of the system model and description of the diesel engine process

The overall propulsion system model is shown in Fig. 2. It includes essential parts of the vessel that interact with each other, namely a vessel hull, a propeller, a mechanical shaft, a diesel engine and a governor, or a speed regulator. Among them, the governor does not exchange energy with others, but it plays a crucial role in the transient behavior of the diesel engine and eventually the whole system. Therefore, it should be included as a part of the system. While the diesel engine is

Please cite this article in press as: Yum, K.K., et al., Simulation of a two-stroke diesel engine for propulsion in waves, International Journal of Naval Architecture and Ocean Engineering (2016), http://dx.doi.org/10.1016/j.ijnaoe.2016.08.004

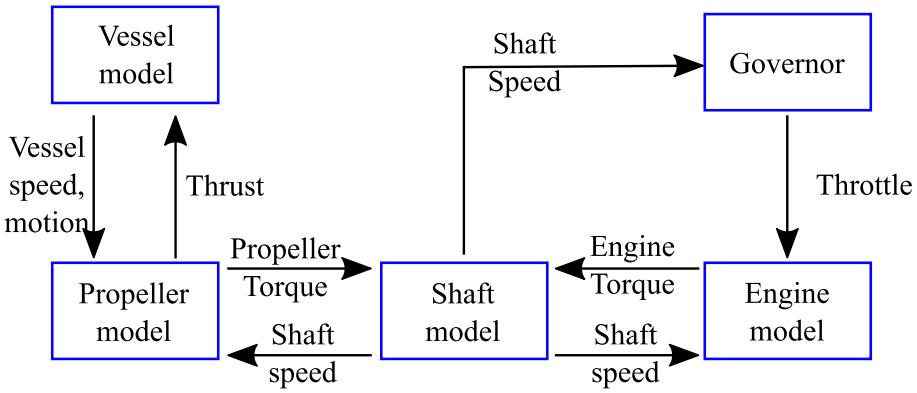

Fig. 2. Schematic of a marine propulsion system.

a technical component of the overall propulsion system, it is also a complex engineering system composed of different sub-components. In order to capture the transient behavior of the system, it should include the essential thermodynamic parts, a torque conversion mechanism (crank mechanism) and control logics. Fig. 3 shows the technical components to be included in the engine system model and the configuration of the system. The arrow in the figure represents the direction of mass and energy flow in the system. A typical turbocharged two-stroke marine diesel engine comprises turbochargers, scavenge air coolers, a scavenge air receiver, a block of cylinder assemblies, pistons and crank mechanism, an exhaust manifold and a receiver, a wastegate and auxiliary blowers. A turbocharger is composed of a compressor located before the inlet of the scavenge air cooler, a turbine placed after the exhaust receiver and a mechanical shaft connecting the two turbomachineries. The main purpose of having the turbocharger is to increase the charge air density without any external power input so that the power density of the diesel engine increases without sacrificing efficiency.

The thermodynamic process starts by taking air into the inlet of a compressor. The air is compressed and becomes hot. In order to increase the density of the air further and prevent excessive temperature in the cylinder, the air is cooled by the scavenge air cooler. Then, the air is collected in a scavenge air receiver which is a large space in the lower part of the engine block. Before the air is taken into the cylinder, the exhaust valve located on the top of the cylinder head opens to expel the combustion gas in the cylinder. As the piston reaches the Bottom Dead Center (BDC), the intake ports located at the lower part of the cylinder wall are exposed to the cylinder volume and the air is drawn into the cylinder. The intake ports are closed, followed by closing of the exhaust valve, as the piston moves upward and the air is compressed during the upstroke of the piston. As the piston reaches to the Top Dead Center (TDC), fuel is injected in a spray form to facilitate vaporizing of fuel and mixing with the charge air. Then, the fuel is auto-ignited and combustion starts while the piston is starting the downstroke. As the piston approaches BDC again, the exhaust valve opens and the combustion gas will start exiting the cylinder through the exhaust manifold to the exhaust receiver. The exhaust gas contains a significant amount of thermal energy, and it drives the turbine to produce torque to run the compressor. Diesel engines are normally equipped with multiple cylinders in order to reduce the torque amplitude and vibration, which comes from the nature of the engine cycle.

A wastegate is a bypass around the turbine, which opens in case of excessive flow of exhaust gas at high engine loads. It is necessary in order to prevent overspeeding of the turbocharger in the cast that the design of the turbocharger is optimized for part load. The auxiliary blowers are turned on when pressure

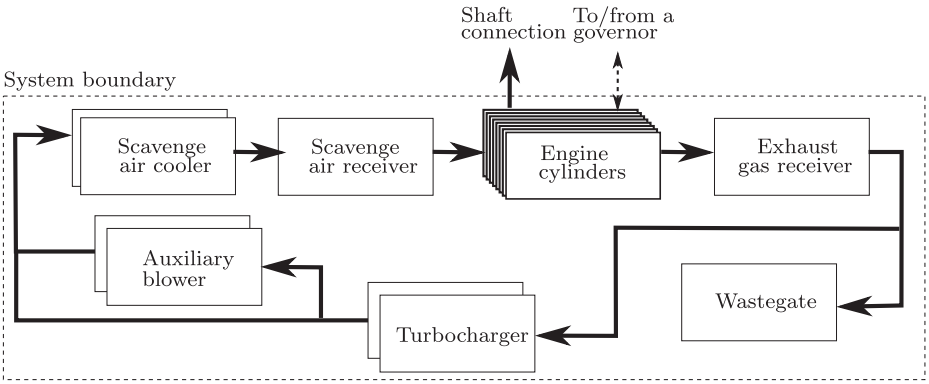

Fig. 3. Schematic of an engine system model.

Please cite this article in press as: Yum, K.K., et al., Simulation of a two-stroke diesel engine for propulsion in waves, International Journal of Naval Architecture and Ocean Engineering (2016), http://dx.doi.org/10.1016/j.ijnaoe.2016.08.004

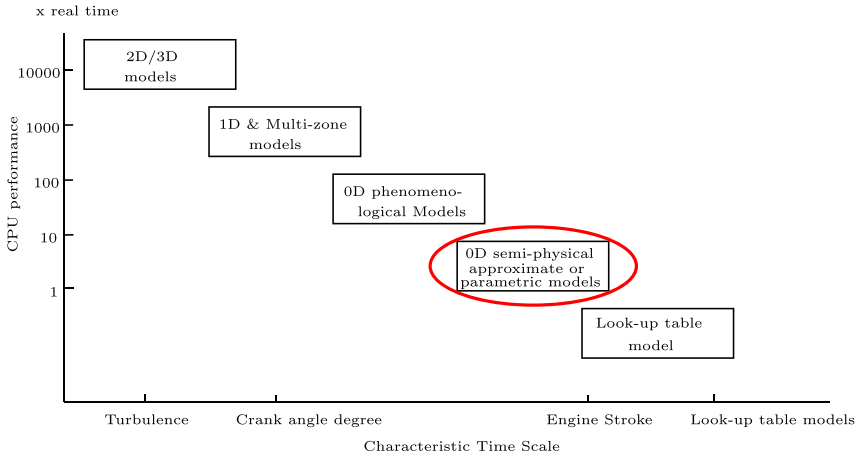

Fig. 4. Computational performance of the combustion modeling framework (Albrecht et al., 2007).

at the scavenge air receiver is lower than a certain value to assist the gas exchange process.

2.3. Selection of submodels

After the scope of the system model is defined, proper models for the physical processes of each component are selected. The selected model should be able to provide the required fidelity and, at the same time, allow the simulation model to run at a reasonable computational speed. In addition, the selected component models should be well-balanced in their fidelity, as the quality of the overall system model is no better than a worst submodel in it (Heywood, 1988, p.750).

For modeling a diesel engines, the most crucial physical process to consider is combustion. The illustration in Fig. 4 by Albrecht et al. (2007) provides an overview of different models for combustion processes, from a look-up table to the CFD model. According to the simulation goals in regards to capturing the transient effect in efficiency and achieving the real-time speed, the proper choice would be a 0D semi-physical approximate model. In this model, the in-cylinder pressure, temperature and gas compositions are calculated in crank angle resolution and the combustion model is prescribed by a parametric Wiebe function.

For the air and exhaust path modeling, a filling and emptying approach (Heywood, 1988, p.754) is used where the momentum of gas flow is not considered. This method is physically appropriate since large two-stroke marine engines are provided with a large volume of scavenging space and an exhaust receiver, thereby, providing relatively constant pressure for gas exchange (Heywood, 1988, p.263). This method is also most commonly used for the engine system simulations in general (Rakopoulos and Giakoumis, 2006).

For modeling turbochargers, the physical process is assumed to be in quasi-steady state where the flow and the isentropic efficiency are determined from a look-up table. It is

Table 1
Selection of physical process models for the engine components.

Components		Process	Submodel
Engine Cylinder	Control volume	Thermodynamic states	0D single zone
		Heat transfer	Convection only
	Scavenge port	Mass flow	Isentropic compressible fluid flow with discharge coefficient
	Exhaust valve	Valve lift	A Look-up table
		Mass flow	Isentropic compressible fluid flow with discharge coefficient
	Crank mechanism	Transformation ($p \rightarrow M$)	Kinematics only
	Combustion	Rate of heat release	Parametric function (Wiebe)
	Scavenging	Scavenging	Empirical model for exhaust gas composition (e.g. S-shape model by Sher (1990))
Turbocharger	Compressor	Mass flow, efficiency	A look-up table
		Compression	Isentropic compression with efficiency considered
	Turbine	Mass flow, efficiency	A look-up table
		Compression	Isentropic compression with efficiency considered
	Shaft	Speed	Single rigid body
Scavenge air cooler		Mass flow	Isentropic compressible fluid with discharge coefficient flow
		Heat transfer	Effectiveness-NTU method
Scavenge air & exhaust gas receiver	Control volume	Thermodynamic state	0D single zone
		Heat transfer	No heat transfer
Wastegate		Mass flow	Isentropic compressible fluid with discharge coefficient flow
Auxiliary blower		Mass flow	A look-up table

Please cite this article in press as: Yum, K.K., et al., Simulation of a two-stroke diesel engine for propulsion in waves, International Journal of Naval Architecture and Ocean Engineering (2016), http://dx.doi.org/10.1016/j.ijnaoe.2016.08.004

a function of the pressure ratio across the turbomachinery and its rotating speed. For flow restriction components such as intake ports, exhaust valves and wastegate, the equation for isentropic compressible gas (Heywood, 1988) is used to model the mass flow.

For the scavenge air cooler, effectiveness-NTU method (Bergman et al., 2007) is used for heat transfer modeling and the isentropic compressible flow equation is used for the pressure drop relation with the air flow. For fuel injection, no physical model is used as the combustion profile is prescribed as a parametric function.

The summary of the selections for the diesel engine system is given in Table 1. Detailed description of the physical sub-models are given in Section 3.

2.4. System variables and interface structure

A good interface structure of interfaces and clear definition of the system variables help to implement the physical process models into the mathematical models and the computerized code. Additional benefits would be the component models built in such a fashion will be easy to reuse in other system models and one can eventually build a model library when the multiple instances of different components are available (Yum and Pedersen, 2016).

The overall propulsion system model shown in Fig. 2 is in a mechanical domain where the system variables are a set of either translational velocity and force or rotational velocity and torque. The component models with inertia like a vessel model and a shaft model have forces/torques as input and give a velocity as an output. The propeller model is a kind of a resistive element which receives the vessel speed or the shaft speed as inputs and produces thrust force to the vessel and torque to the shaft from algebraic relationships. The diesel engine model has a power connection with a shaft where the shaft speed is an input to the model and torque is an output to the shaft. The engine model has additional signal communications with a governor determining the fuel rack position.

Inside the diesel engine model, a complete system model of the thermodynamic process of the diesel engine is enclosed. For the system variables of the thermodynamic process, a vector set of thermodynamic states ($[p, T, F, V]^T$), and another vector set of mass and energy transfer rate or rate of change in a control volume, $[\dot{m}, \dot{E}, \dot{m}_{bf}, \dot{V}]^T$, are used. This approach is inspired by the pseudo-bond graph approach of the thermodynamic modeling (Karnopp, 1979; Pedersen and Engja, 2000). In the components where the volume quantity is fixed, V and $\dot{V}$ can be omitted. The fuel/air equivalence ratio, F, are used to represent the composition of the combustion gas and it is defined as,

$$F = \frac{m_{bf}}{m_a f_s} \tag{1}$$

where m_{bf} is mass of the burned fuel, m_a is mass of air before combustion and f_s is a stoichiometric fuel/air ratio. Given a set of $[p, T, F]^T$, specific quantities of the thermodynamic properties can be obtained, and when the volume quantity is available, the thermodynamic state of the control volume can be determined.

In the proposed scheme by Yum and Pedersen (2016), the components models for the thermodynamic system of a diesel engine can be grouped into two types: flow restriction and flow accumulation. See Sections 3.1.1 and 3.1.2 for more explanation. A flow restriction component has one or more sets of $[p, T, F]^T$ as inputs and $[\dot{m}, \dot{E}, \dot{m}_{bf}]$ an output or outputs, whereas a control volume component has one or more sets of $[\dot{m}, \dot{E}, \dot{m}_{bf}]^T$ as inputs and gives a set of $[p, T, F]^T$ as an output.

For the configuration of the system, the filling and emptying approach is used as a general principle. In this approach, the components belonging to the flow accumulation group are arranged in a series as it would be configured in the real system. These are pipes, plena and in-cylinder volumes. Then a flow restriction element is placed between adjacent control volumes. Turbocharger, ports, valves and cooler components are considered as flow restriction elements. A generic structure is shown in Fig. 5.

When a thermodynamic system is modeled in the suggested scheme, the calculation scheme is straight forward as described below. The numbers in the procedure correspond to the numbers in Fig. 5.

① The thermodynamic states in the control volumes are determined from the state values of mass of fuel and volume (m, E, m_{bf}, V). The state values are obtained from the initial values or integration of the net flow values of them.
② The thermodynamic states of the control volumes are fed to the connected flow restrictions. For those having variable volumes, the pressure is given to the mechanical connection.
③ In the flow restriction components, the flows of energy and mass are determined for each connected control volumes depending on the thermodynamic states of the connected control volumes.
④ The flows of mass and energy are fed back to the connected control volumes. For those having variable volume, the rate of volume change is fed back as response to the pressure given in step 2. Repeat from 1.

3. Description of the submodels

In this section, the physical models, selected in the previous section, will be explained in more detail with mathematical descriptions.

3.1. Diesel engine system

Before presenting the physical models for specific components, two generic elements are explained: flow accumulations and flow restrictions. As discussed in Section 2.4, all the component models will fall under these two categories.

Please cite this article in press as: Yum, K.K., et al., Simulation of a two-stroke diesel engine for propulsion in waves, International Journal of Naval Architecture and Ocean Engineering (2016), http://dx.doi.org/10.1016/j.ijnaoe.2016.08.004

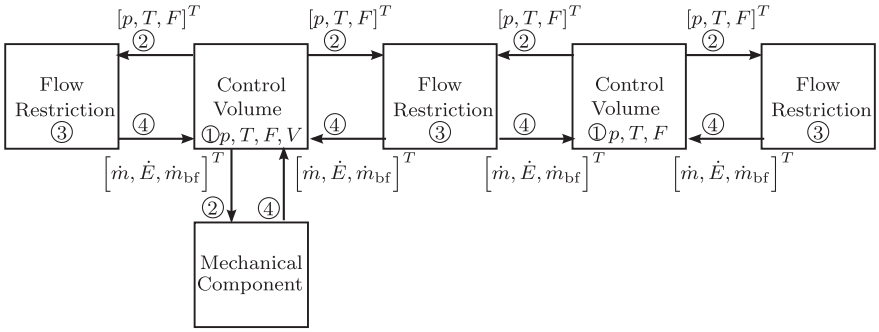

Fig. 5. Schematic of the system configuration and interface structure.

3.1.1. The flow accumulation group

In a component belonging to this group, mass, energy and gas species are accumulated, and, thereby, the thermodynamic states are determined. Such physical components are pipes, plena and in-cylinder volumes. They are often referred to as control volumes.

The governing laws for control volumes are the mass and energy conservation law and the ideal gas law. In addition, a semi-empirical correlation between $[p,\ T,\ F]^T$ and the thermodynamic properties, proposed by Zacharias (1967) is used. A control volume model consists of two parts: a flow junction and an internal volume. In the flow junction, the net rates of change of mass ($\dot{m}_{cv}$), internal energy ($\dot{E}_{cv}$) and mass flow of burned-fuel ($\dot{m}_{cv,bf}$) are calculated by the mass and energy balance from the flow inputs of the connected flow restrictions. In the internal volume, the resulting rates of change are integrated to give mass, internal energy and mass of burned fuel. In case of varying volume, the rate of volume change is also integrated to find the volume quantity of the control volume.

$$\begin{aligned} m_{cv} &= \int \sum_i m_i dt \\ U_{cv} &= \int \dot{Q} - \dot{W} + \sum_i \dot{m}_i h_i dt \\ m_{bf,cv} &= \int \sum_i m_{bf,i} dt \\ V_{cv} &= \int \dot{V}_{cv} dt \end{aligned} \tag{2}$$

From the given states in the equation, the system of the following nonlinear equations are solved iteratively.

$$\begin{aligned} u_{cv} &= u(p,T,F) \\ pV_{cv} &= m_{cv}RT \\ F &= \frac{m_{cv,bf}}{(m_{cv}-m_{cv,bf})f_s} \end{aligned} \tag{3}$$

3.1.2. The flow restriction group

A flow restriction component determines the flows of mass and energy between control volumes depending on their thermodynamic states. Valves, ports, charge air coolers, compressors and turbines fall into this category. In many instances, the following isentropic flow equation for compressible gas is used for a flow restriction element.

$$\dot{m} = \frac{C_D A_T p_{in}}{\sqrt{R_{in} T_{in}}} \Pi \tag{4}$$

where,

$$\Pi = \begin{cases} \left(\frac{p_{out}}{p_{in}}\right)^{1/\gamma} \left\{ \frac{2\gamma}{\gamma-1} \left[1 - \left(\frac{p_{out}}{p_{in}}\right)^{\gamma-1/\gamma} \right] \right\}^{1/2}, & \frac{p_{out}}{p_{in}} < \left(\frac{2}{\gamma+1}\right) \\ \gamma^{1/2} \left(\frac{2}{\gamma+1}\right)^{\gamma+1/2(\gamma-1)}, & \text{otherwise} \end{cases}$$

where, $\dot{m}$ is mass flow across the restriction and A_T is geometrical area of the restriction. For a specific application, C_D and A_T can be either fixed parameters or variables that depend on the pressure ratio, the opening ratio or crank angle.

For energy flow, the conservation of energy is applied as expressed in the following equation.

$$\begin{aligned} \dot{E}_{in} &= \dot{m} h_{in} \\ \dot{E}_{out} &= \dot{E}_{in} - \dot{Q} - \dot{W} \end{aligned} \tag{5}$$

3.1.3. The cylinder assembly model

A cylinder assembly model consists of sub-components and a number of physical process models to describe the thermodynamic cycle of the engine. In this work, the main components to be included are an in-cylinder control volume, intake ports, an exhaust valve and crank mechanism. Physical process models required for the component models are a combustion model, a heat transfer model and a scavenging process model. The structure of the cylinder assembly model is shown in Fig. 6. The diagram shows only the main system variables. There are other signal connections such as a fuel rack position, a fuel injection timing and the crank angle information.

The combustion model. The combustion model is used as an a heat source to the in-cylinder control volume. In this work, three Wiebe functions are used to describe the Rate of Heat Release (ROHR) during combustion (Ghojel, 2010). The Start of Combustion (SOC) (φ_{ig}) is determined by predefined injection timing (φ_{inj}) and the ignition delay (φ_{id}).

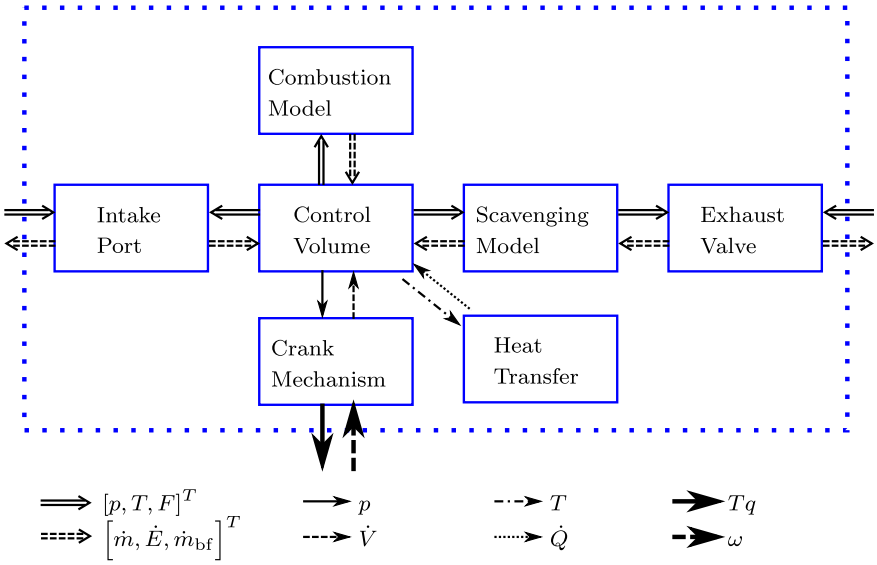

Fig. 6. A cylinder assembly model.

$$\varphi_{\mathrm{ig}} = \varphi_{\mathrm{inj}} + \varphi_{\mathrm{id}} \tag{6}$$

The ignition delay can be calculated according to a semi-empirical expression (Heywood, 1988):

$$\varphi_{id} = \frac{180}{\pi}\omega A \exp\left(\frac{E_A}{\overline{R}T_{\mathrm{cyl}}}\right) p_{\mathrm{cyl}}^{-n} \tag{7}$$

where

E_A: Apparent activation energy for the fuel autoignition process (J mol^{-1})
$\overline{R}$: Universal gas constant (J K^{-1} mol^{-1})
T_{cyl}: Mean cylinder temperature (K)
p_{cyl}: Mean cylinder pressure (bar)
A, n: Constants dependent on the fuel

According to Wolfer (Heywood, 1988), fuel with ceptane number greater than 50 will have $n = 1.19$, $A = 0.44$ and $E_A/R = 4650$.

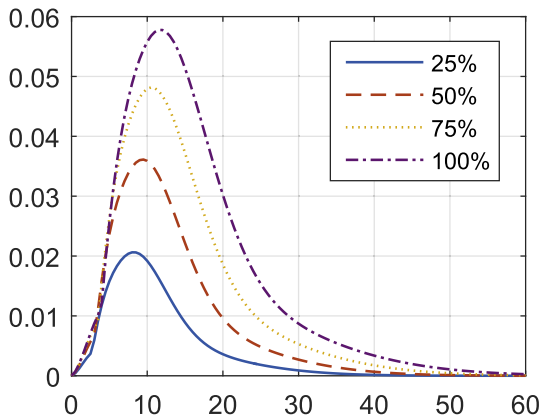

Fig. 7. ROHR for different amount of fuel injection (Normalized).

An actual ROHR profile depends on many factors such as shaft speed, engine load, air flow, intake pressure and temperature, cylinder wall temperature and more to name. The parameters for Wiebe functions may be correlated to these factors in order to achieve a true transient combustion model. Being a Multiple-Input-Multiple-Output (MIMO) relation, it requires a large amount of reference data and an extensive process of curve fitting to find such a model.

In this work, such reference data were not available. Therefore, a transient combustion model could not be developed. Only a single fixed ROHR curve was applied for all conditions instead. However, the combustion duration was varied according to the amount of fuel injected as shown in Fig. 7. This limits the capability of the model to predict the transient performance to a certain degree but it was found that the effect of the exhaust valve timing and the fuel injection timing were dominant in determining the efficiency of the cycle. In conclusion, the application of a single combustion profile still provides acceptable validity of the model in terms of efficiency prediction under transient load condition. This will be shown in Section 4.

The heat transfer model. The main heat transfer model used in this work is one proposed by Eichelberg (Finol and Robinson, 2006) given as following equation.

$$\begin{aligned} \dot{Q}_{\mathrm{w}} &= kA\left(T_{\mathrm{gas}} - T_{\mathrm{w}}\right) \\ k &= \alpha_{\mathrm{ht}} C_m^{1/3} \left(p_{\mathrm{Cyl}} T_{\mathrm{Cyl}}\right)^{1/2} \end{aligned} \tag{8}$$

A is area of heat transfer and T_{gas} and T_{w} are temperature of the gas in the cylinder and the wall in contact, respectively. α_{ht} is used as an correlation factor to the specific application. T_{w} is assumed to be uniform for all surrounding body and found from the heat balance for the lump body of the cylinder.

$$T_{\mathrm{w}} = \frac{1}{m_{\mathrm{cyl}} C_{p,\mathrm{cyl}}} \int \dot{Q}_{\mathrm{w}} - \dot{Q}_{\mathrm{cool}} dt \tag{9}$$

Please cite this article in press as: Yum, K.K., et al., Simulation of a two-stroke diesel engine for propulsion in waves, International Journal of Naval Architecture and Ocean Engineering (2016), http://dx.doi.org/10.1016/j.ijnaoe.2016.08.004

$\dot{Q}_{cool}$ is empirical function in T_w found from the steady state simulation.

Intake ports and an exhaust valve. Intake ports are located on the lower part of cylinder wall along the circumferential. When the piston is passing these holes downward, the air in the scavenging space are blown into the cylinder. The mass flow can be modeled using the isentropic compressible flow Eq. (4) and the opening is a function of the piston position. The discharge coefficient for the flow restriction model is provided using the correlation suggested by Benson and Pool (1965).

For the exhaust valve, the valve actuation mechanism is not modeled but the valve lift is given by the prescribed function of crank angle. The valve lift is composed of three operating phases: opening, lifted and closing. By changing the lifted duration, one can control the Exhaust Valve Close (EVC) timing, which has a major influence on the cycle efficiency and the maximum cylinder pressure. Opening area of the gas passage is calculated from the geometrical dimension of the valve and the port and the valve lift (Heywood, 1988, p. 220). The mass flow is also modeled using the flow Eq. (4) and the discharge coefficient is correlated to the opening fraction and pressure ratio across the valve (Annand and Roe, 1974). The temperature and the composition input from the cylinder side has to be modified from what are directly obtained from the in-cylinder control volume due to the scavenging effect. See the next paragraph for the scavenging model. Fig. 8 shows the profile used for the valve and the calculated area of the port and valve opening depending on the crank angle in normalized quantity.

A scavenging process model. In two stroke diesel engines, expulsion of the combustion gas out of the combustion chamber and intake of fresh air charge happen simultaneously. Among different methods of scavenging, uniflow scavenging is most commonly used in the marine two-stroke diesel engines for its highest efficiency. In this process, the exhaust valve on the top of the cylinder opens first letting the combustion gas escape the combustion chamber. When the piston moves further down and exposes the intake ports to the in-cylinder volume, the charge air from the scavenging receiver will enter the cylinder volume. Ideally the fresh charge will displace the combustion gas upward, so eventually it will fill up the cylinder volume. In reality, some of the charge air is mixed with the combustion gas or even there is short-circuit flow of air directly to the exhaust receiver. In order to maximize the displacement effect, the inward flow of the charge air is directed to the wall side, creating swirl. See Fig. 9 for the illustration of the process.

Even though this is a complex three-dimensional flow process, many researchers have suggested empirical models to describe the process. Sher's paper (Sher, 1990) provides a good summary of those models. Among others, we chose Sher's S-type model for this gas exchange process. In this model, a cylinder volume is divided into two zones: burned and unburned zones. In each zone, the gas is perfectly mixed that the thermodynamic properties are uniform. Intake air enters into the unburned zone and some of air in the unburned zone will be mixed into the burned zone. The mixing process is specified by an empirical function for the mass fraction of fresh charge air content in the gas passing through the exhaust port. First, the mass fraction of fresh charge air content (β_{scav}) is defined as

$$\beta_{scav} = \frac{\dot{m}_{in}}{\dot{m}_{in} + \dot{m}_{exh,cyl}} \tag{10}$$

where m_{in} is mass of fresh air charge which is mixed with the combustion gas, $m_{exh,cyl}$ is mass of the combustion gas from the cylinder. According to Sher's model (Sher, 1990), β_{scav} can be also empirically correlated to the delivery ratio (λ_s) as follows:

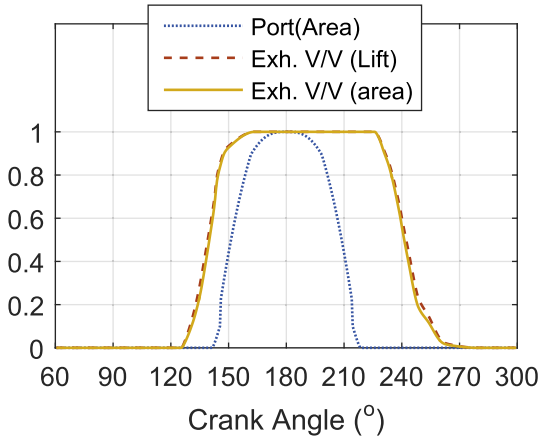

Fig. 8. Normalized opening area of an intake port and an exhaust valve and valve lift profile.

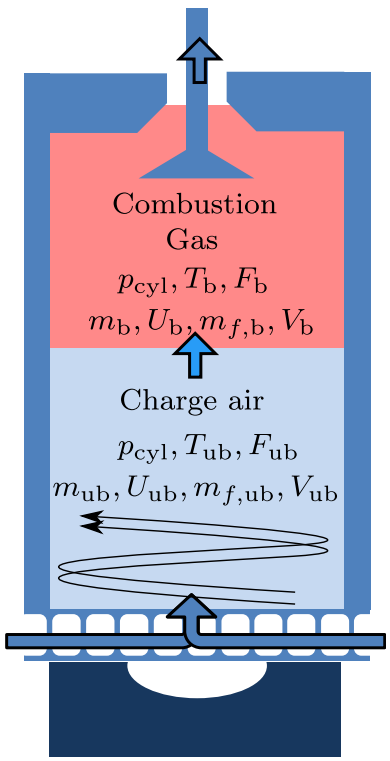

Fig. 9. Uniflow scavenging of a two-stroke diesel engine.

Please cite this article in press as: Yum, K.K., et al., Simulation of a two-stroke diesel engine for propulsion in waves, International Journal of Naval Architecture and Ocean Engineering (2016), http://dx.doi.org/10.1016/j.ijnaoe.2016.08.004

$$\beta_{scav} = 1 - \exp\left(-c\lambda_s \zeta^b\right) \tag{11}$$

where b and c are the form and shape factor respectively, ζ is defined as:

$$\zeta = \frac{\varphi - \varphi_{IPO}}{\varphi_{IPC} - \varphi_{IPO}}$$

The delivery ratio is defined as:

$$\lambda_s = \frac{m_{scav}}{\rho_{scav} V_{disp}} \tag{12}$$

where, m_{scav} is total mass of air that entered the cylinder from the scavenge air receiver, ρ_{scav} is the density of air in the scavenging space and V_D is displacement volume of the cylinder.

Assuming that the fresh air charge is purely air, the fuel/air equivalence ratio of the exiting gas at the exhaust valve can be described with β_{scav} and the initial fuel/air equivalence ratio of the gas in the cylinder before the gas exchange (F_{init}) begins. The derivation of the equation is found in Appendix A.

$$F_{out} = \frac{(1-\beta_{scav})F_{init}}{\beta_{scav}F_{init}f_s + 1} \tag{13}$$

In addition to the composition of the exhaust gas, its temperature has to be determined considering mixing of the fresh air charge in the exhaust gas. The specific enthalpy of the exhaust gas at the valve outlet is given as following.

$$h_{exh} = \beta_{scav}h_{in} + (1-\beta_{scav})h_{cyl} \tag{14}$$

where h_{in} and h_{cyl} are the specific enthalpy for the fresh charge air from the scavenging volume and for the gas in the cylinder before intake port open (IPO). Then, temperature can be determined from the given set of. (p_{cyl}, h_{exh}, F_{out})

Crank mechanism. A crank mechanism transforms the rotating energy of the crank shaft to the linear translation energy of the piston. In this work, only kinematic relation is considered and all the inertia is added to the crank shaft as a single rigid body. All the friction will be modeled as a single bearing on the crank shaft as well. The schematic of the crank mechanism is shown in Fig. 10. Then, the kinematic relation is given as in the following equation.

$$M = e \cdot F_p \quad \dot{x}_p = e \cdot \omega_{eng} \tag{15}$$

where M is the transformation modulus given as

$$e = -a\left(\sin\varphi + \frac{2\lambda\sin 2\varphi}{\sqrt{1-(\lambda\sin\varphi)^2}}\right) \tag{16}$$

where a is the length of the crank arm and λ is ratio of a to the length of connection rod(l).

3.1.4. A turbocharger, a wastegate and an auxiliary blower

The thermal part of the turbochargers is modeled as a flow restriction component. In the model, corrected mass flow ($\dot{m}_{corr}$) and isentropic efficiency (η_{is}) of the machine are found from the performance map with given pressure and temperature of the adjacent control volumes and the rotor speed as inputs.

$$[\dot{m}_{corr}, \eta_{is}] = \Phi_{map}(p_{in}, p_{out}, T_{in}, n_{tc}) \tag{17}$$

Since the input and output of performance map is given in the corrected values, it has to be converted to the real values.

In the calculation of energy flow using Eq. (5), heat transfer is neglected, and the rate of work done to the turbocharger shaft can be calculated using the obtained isentropic efficiency.

$$\dot{W}_{comp} = \frac{\Delta h_{is}}{\eta_{comp}} \quad \dot{W}_{turb} = \Delta h_{is}\eta_{turb} \tag{18}$$

where, the enthalpy change of the isentropic process (Δh_{is}) can be obtained by:

$$\Delta h_{is} = h_{is,out}(p_{out}, T_{is,out}, F_{in}) - h_{in}(p_{in}, T_{in}, F_{in}) \tag{19}$$

and the isentropic temperature (T_{is}) can be calculated assuming the expansion or the compression is isentropic process. Then, the shaft torque produced or consumed by the turbomachinery is given as follows:

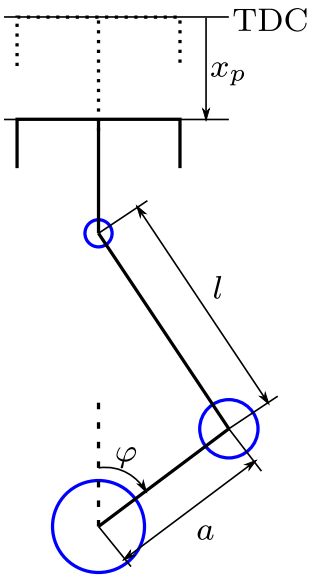

Fig. 10. Crank mechanism.

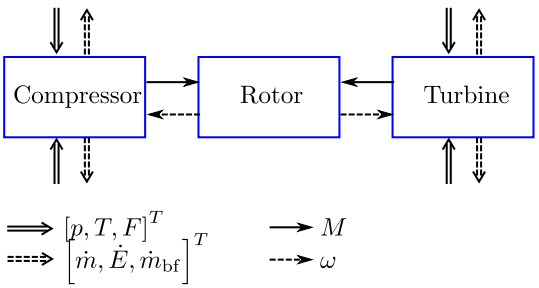

Fig. 11. A turbocharger model.

$$M = \dot{W}/n_{tc} \tag{20}$$

A rigid-body shaft model is used for dynamics of turbocharger rotor. Then, the dynamic equation is given as follows:

$$J_{tc}\dot{n}_{tc} = M_{turb} - M_{comp} \tag{21}$$

No friction is shown in the equation since it is included in the efficiency of the turbine. The structure of the turbocharger model is shown in Fig. 11.

An auxiliary blower is an electrically driven machine which is turned on when the engine load and its speed are lower than a certain level, typically 30% of rated power with a propeller load. Below this load, the turbocharger is not capable of delivering sufficient air for the scavenging process, and, therefore, the blower assists the air supply. A blower of centrifugal type is commonly used with an induction motor running at a fixed speed. In the air path, the blower is located after the scavenge air cooler and the outlet is connected to the scavenge air receiver. When the blower is not in operation, air from the scavenge air cooler will enter directly into the scavenge receiver through a non-return flaps valve. When the blower is turned on, the flap valve is closed by the negative pressure at the suction of the blower and all the air enters the scavenge air receiver through the blower. On-and-off switching is done by a hysteresis controller which receives the signal of pressure in the scavenge air receiver. As the blower is a fixed speed compressor, it can be modeled in a similar but simpler way as the compressor. Only a single curve for each flow and efficient in function of pressure ratio is sufficient. The rest of the calculation is identical to the compressor for the turbocharger.

A wastegate is a bypass configuration with a control valve around the turbine. The control valve is opened by a hysteresis control when pressure at the scavenge air receiver is higher than a preset value. There is also a flow controller that maintains the bypass flow at the preset fraction of the total exhaust gas flow. It is modeled as an ideal nozzle by the flow Eq. (4) with variable effective area that is controlled by a wastegate controller.

3.1.5. A scavenge air cooler

The scavenge air cooler cools the air going into the engine cylinder so that the air is dense enough to achieve higher power. As a simplification, it can be viewed as a flow restriction element with heat transfer. Knowing the maximum flow rate of the gas and the corresponding pressure drop, the effective area of air passage as a simple nozzle can be calculated from (4).

For the heat transfer part, an effectiveness-number-of-transfer ($\varepsilon - NTU$) model is used (Bergman et al., 2007) and the heat transfer coefficient for the cross-flow can be found from the following semi-empirical formulation developed by Churchill and Bernstein (1977). It should be noted the heat conductivity of the pipe and the coefficient of heat convection of the cooling water side are neglected since the values are small compared to convection of the hot gas.

$$k = \frac{\lambda}{D_{pipe}}\left\{0.3 + \frac{0.62\mathrm{Re}_D^{1/2}\mathrm{Pr}^{1/3}}{\left[1+(0.4/\mathrm{Pr})^{2/3}\right]^{1/4}}\left[1+\left(\frac{\mathrm{Re}_D}{282000}\right)^{5/8}\right]^{0.8}\right\} \tag{22}$$

where,

$$\mathrm{Re}_D = \frac{c_a D_{pipe}\rho_a}{\mu_a} \quad \mathrm{Pr} = \frac{\mu_a Cp_a}{\lambda_a}$$

and μ_a, c_a and λ_a are dynamic viscosity, velocity of the flow and thermal conductivity of the air, respectively.

The area of heat exchange and the pipe diameter are main parameters which can be fitted with the given performance data. Once effectiveness, ε is found, the temperature of outlet gas can be determined and finally the enthalpy of the outlet gas (h_{out}) can be obtained giving the energy flow out of the cooler ($\dot{m}h_{out}$).

3.1.6. Engine controllers

Engine controllers are not a part of the physical system but they affect the system dynamics of the diesel engine in a great deal. In this work, two controllers will be described: a speed governor and a controller for fuel injection and valve timing.

The speed governor and the smoke limiter. A speed governor is a physical or logical device that keeps the shaft speed to a set point by regulating the amount of fuel injections. In this work, a PI controller with saturation and anti-windup control is used. The control law is given by the following equation.

$$\begin{aligned}
&\tilde{e} = \overline{\omega}_{eng,ref} - \overline{\omega}_{eng} \\
&uGov_{pi} = K_p\tilde{e} + \int \frac{K_p}{\tau_i}\tilde{e} - \frac{1}{\tau_a}\left(uGov_{pi} - uGov\right)dt \\
&uGov = \begin{cases} uGov_{max}, & uGovpi > uGov_{max} \\ uGov_{min}, & uGov_{pi} > uGov_{min} \\ uGov_{pi}, & \text{otherwise} \end{cases}
\end{aligned} \tag{23}$$

where $uGov$ is an output of the governor, K_p is a proportional gain, τ_i is a time constant for the integral term, τ_a is a time constant for a anti-windup control. The measured shaft speed of the engine contains high frequency speed variations due to the variation of torque within a engine cycle. It is not desired for this high frequency response to enter the control loop, so the measured signal is low-pass filtered. In this work, a fourth order butterworth filter is used. One challenge with such a filter is that filtered signal lags the actual value in time, and, therefore, one needs to carefully choose a proper bandwidth for the filter.

A smoke limiter is another limiting logic that ensures that the fuel/air mixture is not richer than a preset level. It is done by computing the expected mass of air trapped in the cylinder (m_{tr}) and limit the fuel injection by:

Please cite this article in press as: Yum, K.K., et al., Simulation of a two-stroke diesel engine for propulsion in waves, International Journal of Naval Architecture and Ocean Engineering (2016), http://dx.doi.org/10.1016/j.ijnaoe.2016.08.004

$$uGov_{\text{smoke}} = \begin{cases} \dfrac{m_{\text{tr}} F_{\max} f_s}{m_{f,\text{cyc,max}}}, & uGov > \dfrac{m_{\text{tr}} F_{\max} f_s}{m_{f,\text{cyc,max}}} \\ uGov, & \text{otherwise} \end{cases} \tag{24}$$

where, $m_{f,\text{cyc,max}}$ is maximum amount of fuel injection per cycle and $F_{\max}$ is maximum allowed fuel/air equivalence ratio.

Fuel injection and valve timing. The fuel injection and valve timing are two major factors contributing to the cycle efficiency and the maximum cylinder pressure. Therefore, these timings should be set at the optimal values in the given operation conditions. From the work of Yang and Wang (2013), the injection timing can be related to the shaft speed, the scavenge air pressure and the fuel injection pressure. For example, the injection timing can be calculated by the following relation.

$$\varphi_{\text{inj}} = \varphi_{\text{inj,std}} + \Delta\varphi_{\text{scav}} + \Delta\varphi_{\text{n}} + \Delta\varphi_{p_{\text{rail}}} \tag{25}$$

where, $\varphi_{\text{inj,std}}$ is a standard injection angle before correction, $\Delta\varphi_{\text{scav}}$ is a correction term depending on the scavenge air pressure, $\Delta\varphi_{\text{n}}$ is a correction term depending on the engine speed and $\Delta\varphi_{p_{\text{rail}}}$ is a correction term depending on the fuel rail pressure. In this work, $\Delta\varphi_{p_{\text{rail}}}$ is not accounted for. For the valve timing, we assumed that it is mainly related to the shaft speed. We used a fixed function in shaft speed for the exhaust valve open (EVO) timing, whereas we found the EVC timing values which gives the best match for the measured break specific fuel consumption (BSFC). Then, these points can be interpolated for any shaft speed for transient load simulations.

3.1.7. Crank shaft

A crank shaft is the main shaft of the diesel engine connected to the crank mechanism of each cylinder assembly unit. In our model, the crank shaft is modeled as a rigid body, meaning that the rotational speed is equal to all the cylinder assembly units. It is also a massless node where all the torques produced in the cylinder units are summed, and it gives the net torque as an output. The mass moment of inertia and the friction in this component are added to the shaft model.

3.1.8. Assembly of the engine system model

The assembly of the engine model is a straight forward process since the structure and the interface specifications are clearly described beforehand. The submodels are modularized in a library that an user can configure the system model in the plug-and-play fashion. The detailed overall model of the diesel engine system is shown in Fig. 12. In the figure, a solid double arrow and a dotted one represent the flow of information of $[p,\ T,\ F]^T$ and $[\dot{m}, \dot{E}, \dot{m}_{\text{bf}}]$, respectively. The turbochargers, the scavenge air coolers, the wastegate and the auxiliary blowers are grouped in a submodel, "air/exhaust system". The configuration of these components is shown in Fig. 13. In both figures, a filled circle represents a node where all the outputs are identical to an input and the blank circle is a node where the sum of the inputs are equal to an output. For example, the dotted arrow from the auxiliary blower and the flap valve are connected to the blank circle where the mass and energy flow of these components are added to give the net flow.

We have inserted pipe components before and after the scavenge air cooler in order to comply the interface rules for the components. As the scavenge air cooler, turbocharger and the auxiliary blowers all belong to the flow restriction group, their interfaces are not compatible to each other. Therefore, a flow accumulation component with a small volume quantity can be inserted in between these components without influencing the system dynamics.

3.2. The vessel

We use an one-dimensional dynamic model for the vessel, where we only considered the surge motion of the vessel as below:

$$\left(m_{\text{ship}} + m'\right)\ddot{x} + \left(0.5\rho S C_T \dot{x}^2 + R_1\right) - (1-t)F_T = 0 \tag{26}$$

where m_{ship} is mass of the ship, m' is added mass for the surge motion, x is surge displacement, F_T is thrust produced by the propeller, t is a thrust deduction fraction, ρ is the density of seawater, S is wetted surface area of the ship, C_T is a resistance coefficient of the ship modeled as a function of ship speed. R_1 consists of zero and first order added resistance in waves. Due to the lack of knowledge of variations of the thrust deduction in waves, it has been assumed constant. R_1 is a time dependent input and F_T is given from the propeller model.

In addition, in order to estimate the propeller inflow velocity in waves, periodic surge, pitch and relative stern motions have to be calculated using ship motion RAOs. Ship motion RAOs were calculated using linear strip theory, utilizing potential theory and pressure integration, implemented in the ShipX Veres software developed by MARINTEK. Using the motion response of the vessel, added resistance coefficients were computed using the method by Loukakis and Sclavounos (1978) (which is an extension of the classical Gerritsma and Beukelmans method) implemented in ShipX Veres. Added resistance was then computed in irregular waves for different peak frequencies and wave directions, using the Pierson Moskowitz wave spectrum.

3.3. Propeller and shaft model

An one-quadrant propeller model has been used where the propeller curves of the thrust and the torque coefficients (K_T, K_Q) were obtained using an open-source program, Openprop, based on vortex lattice lifting line theory, along with Javafoil (Hepperle, 2007) to calculate the frictional drag. The torque and the thrust can be calculated from the following equations.

$$\begin{aligned} F_T &= K_T \rho_{\text{sw}} n^2 D_{\text{Prop}}^4 \beta \\ M_{\text{prop}} &= K_Q \rho_{\text{sw}} n^2 D_{\text{Prop}}^5 \beta^{0.8} \end{aligned} \tag{27}$$

where, n is rotational speed of the propeller in rev/s and D_{prop} is diameter of the propeller and β is a factor used to take into

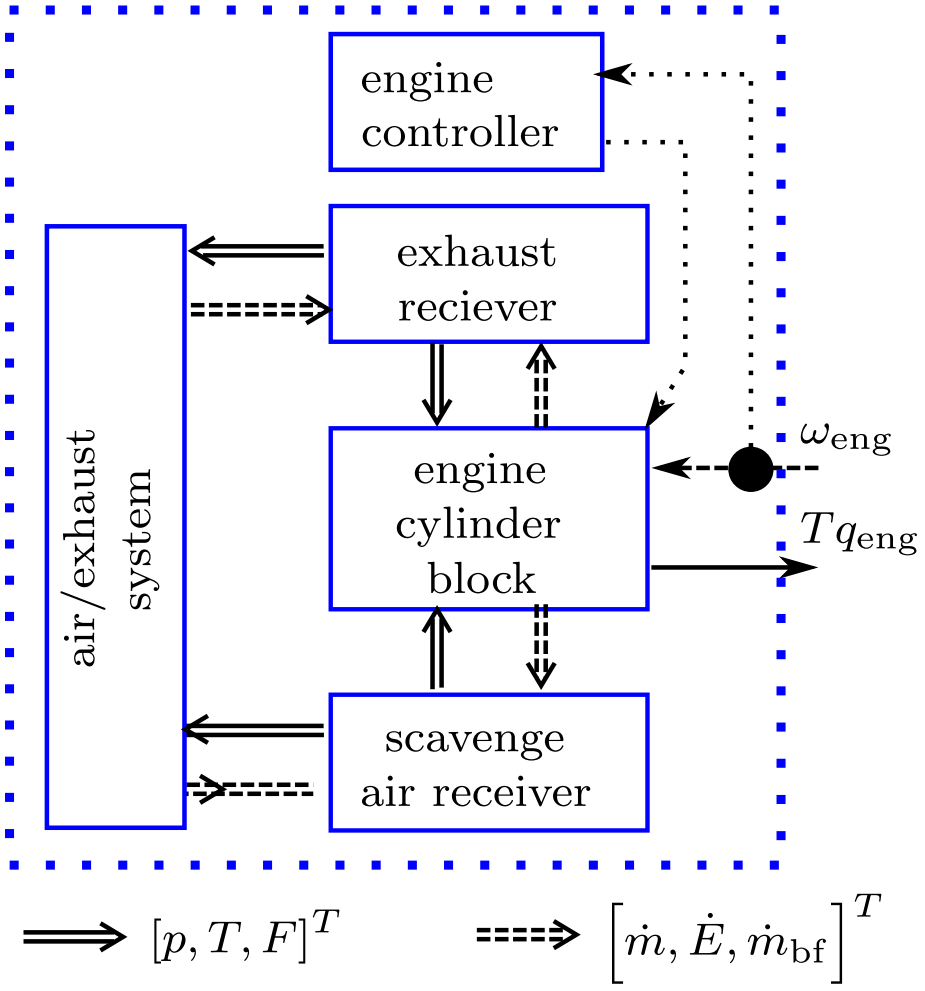

Fig. 12. Configuration of the engine system model.

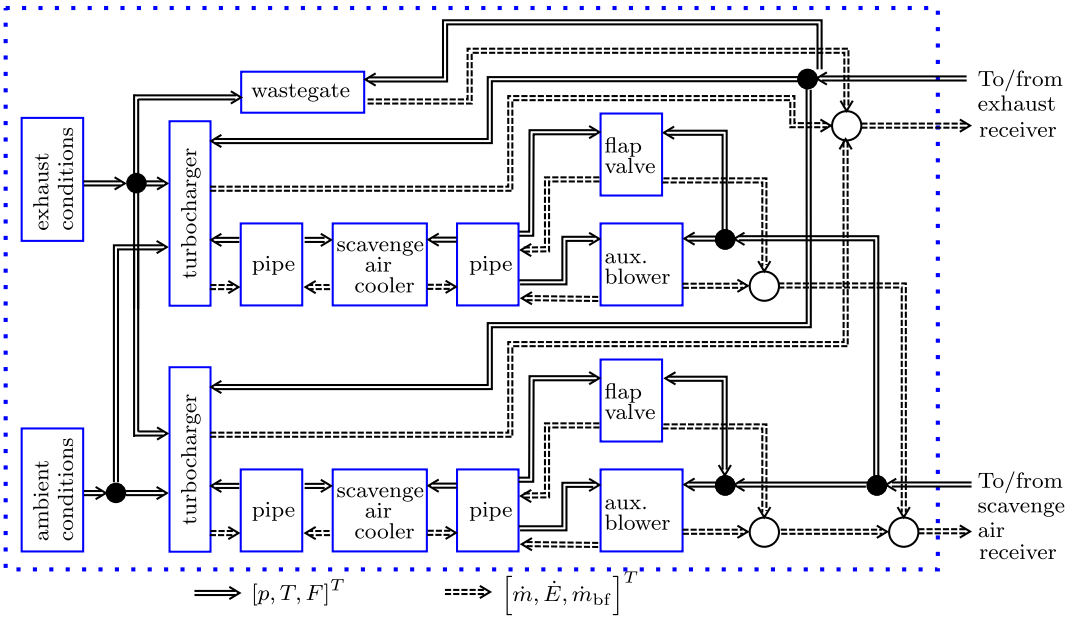

Fig. 13. Configuration of "turbocharging" submodel.

Please cite this article in press as: Yum, K.K., et al., Simulation of a two-stroke diesel engine for propulsion in waves, International Journal of Naval Architecture and Ocean Engineering (2016), http://dx.doi.org/10.1016/j.ijnaoe.2016.08.004

account thrust and torque loss due to the propeller emergence and its proximity to free surface. The value K_T and K_Q are functions in the advance ratio of the propeller, J.

$$J = \frac{v}{nD} \tag{28}$$

where v is the propeller inflow velocity. In order to consider the effect of waves on the propulsion of the ship, thrust and torque losses due to propeller emergence, free surface effect and Wagner effect have been modeled as suggested by Faltinsen et al. (1980) and Minsaas et al. (1983). The effects have been considered in quasi-steady sense as propeller depth varies much slower than its rate of rotation. Thrust and torque are considered varying in wave frequency due to variations of the propeller inflow; higher harmonics have been ignored. The propeller inflow has been calculated considering the effect of waves along with the surge and pitch motion of the ship as follows:

$$\begin{aligned} v = (1-w_p)\{&\dot{x} - \omega_e \xi_a \sin(\omega_e t - \zeta_\xi) \\ &+ \alpha\omega h_a \exp(-kz_p)\cos X \cdot \cos(\omega_e t - kx_p \cos X) \\ &\times\}\sqrt{\left(1 - \frac{\Delta\overline{p}}{0.5\rho\dot{x}^2}\right)} \end{aligned} \tag{29}$$

where w_p is a wake fraction, ω_e is encounter angular frequency, t is time, ζ_ξ is a phase lag of the surge motion, ω is the wave angular frequency, h_a is a wave amplitude, k is a wave number, z_p is the immersion depth of the propeller shaft, x_p is the position of the propeller section with reference to the center of gravity of the vessel, X is wave encounter angle and

$$\alpha = \begin{cases} 0.2\left(\dfrac{\lambda}{L|\cos X|}\right) + 0.5, & \text{for } \dfrac{\lambda}{L|\cos X|} \le 2.5 \\ 1, & \text{for } \dfrac{\lambda}{L|\cos X|} > 2.5 \end{cases}$$

Detailed description of the model can be found in the work of Taskar et al. (2016), which is a complementary work of this paper.

The propulsion shaft is modeled as a single rigid body with friction.

$$J_{\text{tot}}\dot{\omega} + f(\omega) = M_{\text{eng}} - M_{\text{prop}} \tag{30}$$

where, J_{tot} is the mass moment of inertia of the total propulsion system including the main engine crank shaft, a main shaft and a propeller. In the mass term, added mass is ignored for the insensitivity of the value to the overall system response. The second term in the left hand side of the equation is a frictional term, which was approximated as the second order polynomial of the shaft speed.

4. Validation and the sensitivity analysis

The case model we selected for the study is KVLCC2 with the main engine Wartsila 8RT-FLEX68D. The main reason for the choice of the case was availability of the data to validate the model. The main particulars for the vessel, propeller geometry and main engine specifications are given in Table 2. The pitch of the original KVLCC2 propeller was modified in order to match the engine model.

Table 2
Ship particulars, propeller geometry and main engine specifications.

Ship particulars		Propeller geometry	
Length between perpendiculars(m)	320.0	Diameter(m)	9.86
Length at water line(m)	325.5	No of blades	4
Breadth at water line(m)	58.0	Hub diameter(m)	1.53
Depth(m)	30.0	Rotational speed (RPM)	95
Draft(m)	20.8	A_e/A_o	0.431
Displacement (m3)	312,622	$(P/D)_{\text{mean}}$	0.47
Block coefficient (CB)	0.8098	Skew (°)	21.15
Design Speed (m/s)	7.97	Rake (°)	0

The main engine specifications	
Model	Wartsila 8RT-FLEX68D.
Bore (mm)	680
Rated MCR (kW)	25,040
Speed at rated power (RPM)	95
Stroke (mm)	2720
Mean Effective Pressure (bar)	20
Number of cylinders	8
Turbocharger	2 x ABB A175-L35

4.1. Model validation for the propeller and the vessel

In order to validate the propeller curves obtained from Openprop, they were compared with the experimental open water data of original KVLCC2 propeller design as shown in Fig. 14.

For response amplitude operator (RAO) of the vessel, the calculated surge and pitch RAOs are compared to the experimental work by Wu (2013) in head sea. This comparison can be seen in Fig. 15a and b. The surge motion is slightly overestimated compared to experimental values. In addition, the added resistance, calculated using the method by Loukakis and Sclavounos (1978), is also compared to the experimental work by Wu (2013) as shown in Fig. 16.

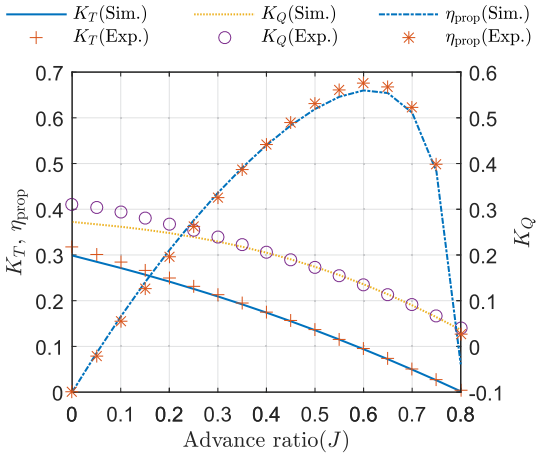

Fig. 14. Propeller curves for KVLCC2 and the experimental result.

Please cite this article in press as: Yum, K.K., et al., Simulation of a two-stroke diesel engine for propulsion in waves, International Journal of Naval Architecture and Ocean Engineering (2016), http://dx.doi.org/10.1016/j.ijnaoe.2016.08.004

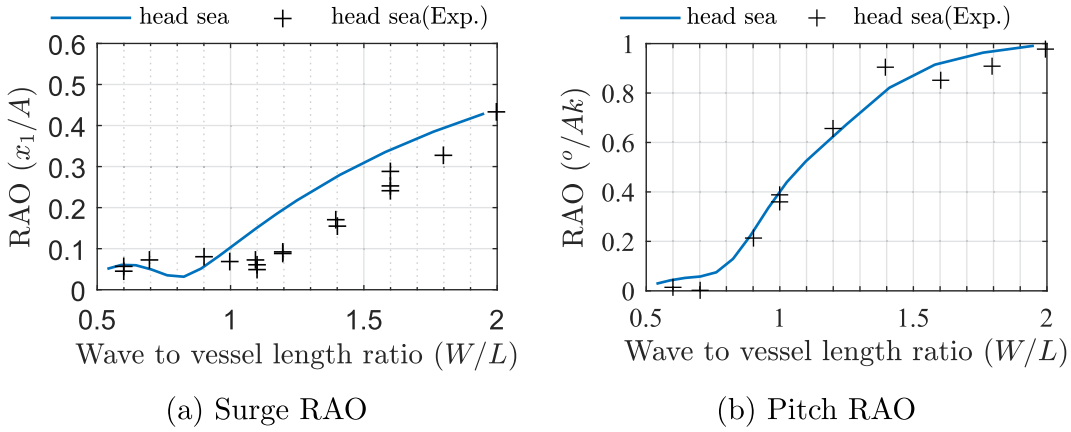

(a) Surge RAO (b) Pitch RAO

Fig. 15. Comparison of the RAO: calculation vs. experiment.

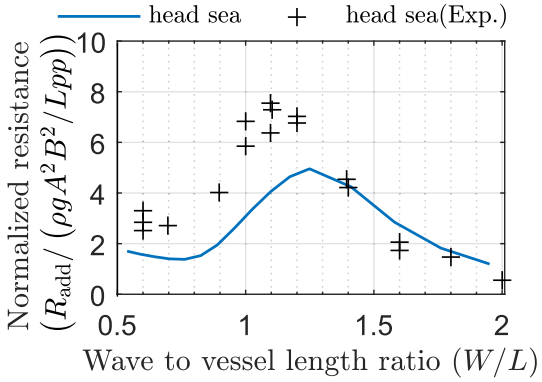

Fig. 16. Comparison for added resistance for head sea.

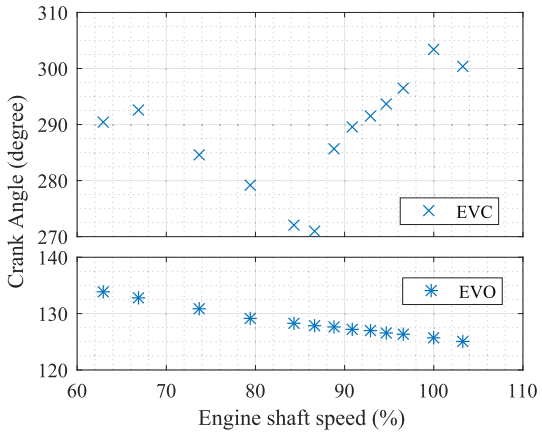

Fig. 17. Exhaust valve timing used for the validation.

4.2. Model validation for the diesel engine

The engine system model was validated against the steady state performance data provided by the engine manufacturer, available on their website (Winterthur Gas and Diesel, 2015). For the steady state simulation, we used a simple propeller-shaft-engine model with a speed governor, where the propeller torque is a quadratic function of the engine speed.

From numerous simulations, we found that BSFC is mainly affected by the EVC timing and the fuel injection timing. Early EVC will make the apparent compression ratio high and lead to better fuel efficiency. Also retarded fuel injection may enable to keep a high compression ratio without exceeding the permissible maximum cylinder pressure. As mentioned in Section 3.1.6, the EVC timing was adjusted during the simulation to match the given BSFC. Fig. 17 shows the EVC timing curve we acquired from the validation process. Having adjusted the EVC timing properly, even though we used fixed shape parameters for the combustion profile, the steady state simulation result matched well with the provided performance data. The result is shown in Fig. 18.

4.3. Sensitivity analysis for transient performance

Sensitivity analysis was done in order to find the dependency of the system model on certain parameters with uncertainty for the transient simulations. When building a simulation model for a diesel engine system under transient operating conditions, it requires an extensive list of parameters, which are mainly describing the physical system and the control system. One can find the parameters for the model against steady-state performance measurements as done in the previous section. However, finding the parameters related to the transient performance is a much more challenging task due to its complexity and the lack of measurements for such a purpose. In addition, acquiring reliable performance data for comparison is also a complicated work due to the transient nature of the sensors and synchronization of the signals. In conclusion, transient performance data are either unavailable or with greater uncertainties compared to the steady state measurement. In this paper, no transient measurements were available for the selected engine model and, therefore, only a qualitative study is carried out.

The parameters related to the transient performance with high uncertainty are listed as below.

- Control gains for the engine speed governor (K_p)
- Cut-off frequency for low pass filter of speed signal (f_{LP})

Please cite this article in press as: Yum, K.K., et al., Simulation of a two-stroke diesel engine for propulsion in waves, International Journal of Naval Architecture and Ocean Engineering (2016), http://dx.doi.org/10.1016/j.ijnaoe.2016.08.004

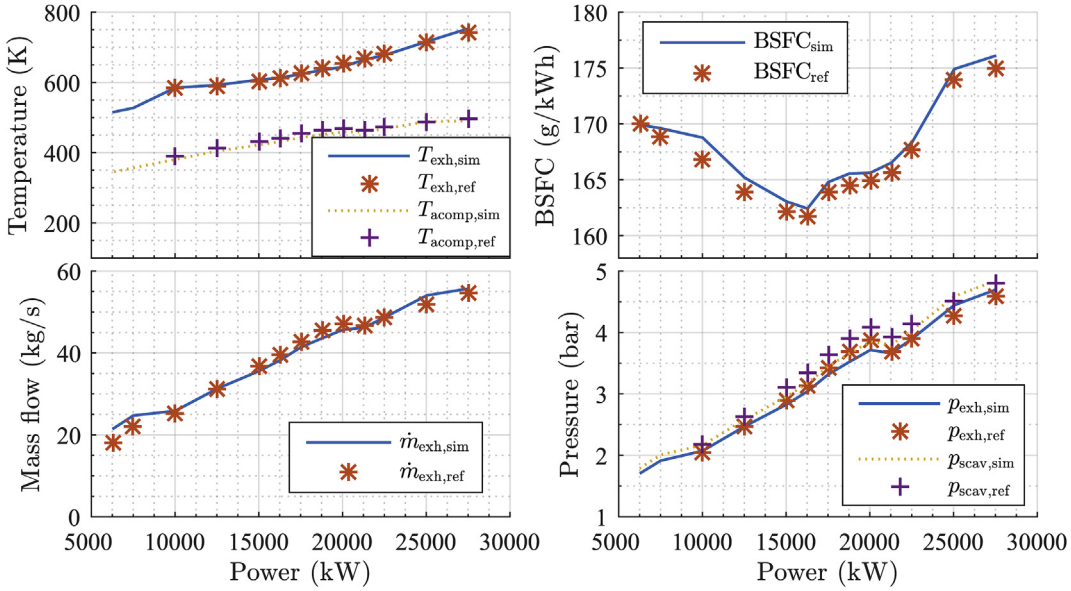

Fig. 18. Validation of the engine system model against steady state performance data.

- Rotational inertia of turbocharger (J_{tc})
- Rotational inertia of propulsion system including added mass (J_{prop})

The first two parameters are the control design values which can be easily adjusted during the design process, whereas the last two parameters are the physical values which are more or less fixed for a given engine model or a propulsion system. However, often only approximate values for these last two are available. Furthermore, there will be a time-varying added inertia due to the hydrodynamic effect of propeller, which adds more uncertainty to the inertia of the propulsion system. Therefore, it is worthwhile to see the influence of these parameters to the system response.

For transient simulation, step load tests were carried out where the set point for the governor was changed from an initial value to a new value in a step. The correlation between the parameters and time constant plus the behavior of the speed response of the diesel engine was studied. The step changes given in Table 3 will be under consideration.

We used a design of experiment method for the analysis where a full factorial test of three levels for each parameter, resulting in 81 experiments, was carried out. The range of the values for parameters is shown in Table 4. The performance index in this case is the time constant (τ_{step}) of the speed change, existence of oscillation of the speed during or after the step response and the maximum value of fuel/air equivalence ratio in the cylinder after combustion.

Table 3
Step load for sensitivity test.

	Initial		Final	
	Power (%MCR)	Speed (RPM)	Power (%MCR)	Speed (RPM)
Case 1	40	70.0	100	95.0
Case 2	70	84.4	100	95.0

Table 4
Range of values for parameters in step response.

	Low	Middle	High
K_p	0.1	1.0	10.0
f_{LP}(Hz)	0.1	1.0	10.0
J_{prop}(kg m^2)	161,500	323,000	646,000
J_{tc}(kg m^2)	1.77	5.30	15.9

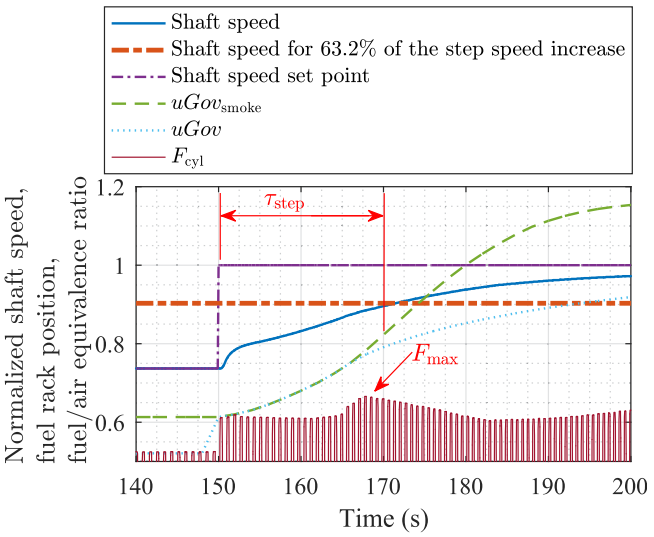

Fig. 19. Step response of the diesel engine with the propeller load (K_p = 1, f_{LP}=1, J_{prop} = 323000 kg m^2, J_{tc} = 5.30 kg m^2).

One case of the simulations is shown in Fig. 19. In this case, the governor output ($uGov$) jumps to a higher value at the sudden change in the set point. Then, it is saturated by the maximum allowable value set by the smoke limiter ($uGov_{smoke}$) until 166.7 s and the system response is delayed while keeping the combustion under lean conditions

Please cite this article in press as: Yum, K.K., et al., Simulation of a two-stroke diesel engine for propulsion in waves, International Journal of Naval Architecture and Ocean Engineering (2016), http://dx.doi.org/10.1016/j.ijnaoe.2016.08.004

($F_{\max} < 0.67$). No oscillation is observed in this case, but it was present after the step is applied in some cases of low J_{prop} and high K_p.

The correlation coefficients between the parameters and the output results are shown in Fig. 20 as a correlation matrix. In terms of the speed response, the mass moment of inertia of the turbocharger rotor has the highest influence whereas the mass moment of inertia of the propulsion system has a negligible correlation. The dominant influence of the turbocharger can be explained by the turbo-lag where the fuel injection is limited by slow development of mass flow due to the inertia of the turbocharger rotor. From the result that the system is not sensitive to inertia of the propulsion system, rough estimation of inertia of the propulsions system can be justified and the added mass of the propeller can be neglected. The control gain has the most influence on the maximum fuel/air equivalence ratio and a certain degree of influence on the speed response. The cut-off frequency of the low pass filter for shaft speed has a small correlation coefficient with all the outputs.

5. Simulation results for various wave conditions

The purpose of the simulation is to observe the system response of the propulsion system and the diesel engine when a vessel is traveling in different wave conditions. In order to do so, following cases with regular waves have been simulated.

- Wave encounter angles (χ_{wave}, °):180, 135, 90, 45, 0
- Wave amplitude (H_{wave}, m): 3, 4, 5
- Wave length (λ_{wave}, m): 192, 352, 512

The reference speed for the propulsion shaft is set to be 88 RPM for all cases.

5.1. System response

As we applied regular waves, all the system responses are periodic, among which most of the results are in the sinusoidal form with the same frequency as the wave encountering frequency. However, some of the results showed irregularity due to different effects in the system. The time series of the main system responses are shown in Fig. 21. The presented time series data except the fuel rack position command are low-pass filtered with a cutoff frequency, 2.5 Hz in order to remove the system response due to the high frequency excitation of the diesel engines. For the convenience of the presentation, we refer the cases as in Table 5.

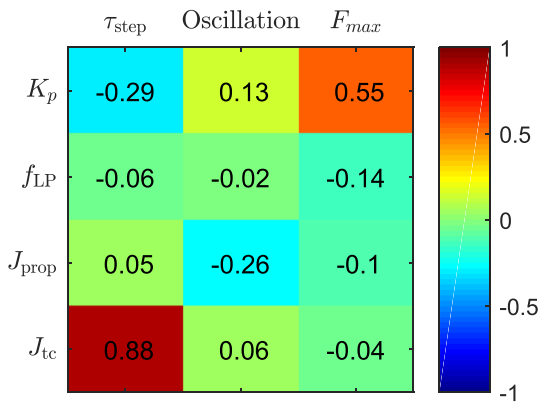

Fig. 20. Correlation matrix for the step response analysis.

In the case A, which is a beam sea condition, the system response is not so much affected by the waves that the performance is similar to the calm water case. In the case B, typical sinusoidal responses are shown in the relatively lower sea state. The vessel speed has decreased due to the added resistance. As the vessel speed slows down, propeller inflow velocity decreases resulting in the increased propeller loading and shaft power accordingly. In both cases, the engine shaft torque is closely catching up with the propeller one with only a small gap. Therefore, shaft speed variation is relatively small.

In the case C, there is a sharp increase in the shaft speed due to emergence of the propeller (① in Fig. 21). During this sharp increase of the speed, the engine power decreases rapidly due to the drop of the propeller torque. Eventually, the shaft speed starts falling as the propeller starts immersing into the water. The speed continues to fall below the set point as the recovery of the engine torque is delayed because of the characteristics of the feedback control system. Finally the speed start increasing toward the set point after the propeller is fully immersed. However, the process is rather slow as the propeller loading increases as the shaft speed accelerates. At some point (② in Fig. 21), the engine output torque is saturated because the governor output has reached the maximum value (1.1 in this work). However, the propeller torque starts decreasing because of change in the inflow velocity due to waves and shaft speed quickly recovers to the set point and overshoots. Then, the propeller start emerging out of water and the cycle starts again.

In the case D, the amplitude of the propeller torque variation is very high due to the large variations of the propeller inflow velocity (③ in Fig. 21). It leads to large periodic system responses in the shaft speed, the shaft power, torques and the thrust. However, the mean power level is relatively lower due to the higher advance ratio. At the lower power level, the output torque is more likely to be limited by the smoke limit control (See Section 3.1.6) as it takes longer to accelerate the turbocharger up to the speed that ensures sufficient air supply. Fig. 22 presents the output of the governor and the maximum limits imposed by the smoke limiter. As seen in the figure, the fuel rack position is limited by the smoke limit control between 116 and 123 s and, therefore, the torque output is limited (④ in Fig. 21). This causes the hollow in the shaft speed (⑤ in Fig. 21) and saturation of thrust.

As far as the engine system response is concerned, the same pattern of responses as the overall system are observed. However, further delays are observed in the scavenging pressure development as well as the turbocharger speed. This is caused by the both mass moment of inertia of the turbocharger and capacitance of the control volume. The typical delayed time is 2–4 s.

The maximum cylinder pressure tends to be higher than what we observed in the steady state simulations. This is caused by the

Please cite this article in press as: Yum, K.K., et al., Simulation of a two-stroke diesel engine for propulsion in waves, International Journal of Naval Architecture and Ocean Engineering (2016), http://dx.doi.org/10.1016/j.ijnaoe.2016.08.004

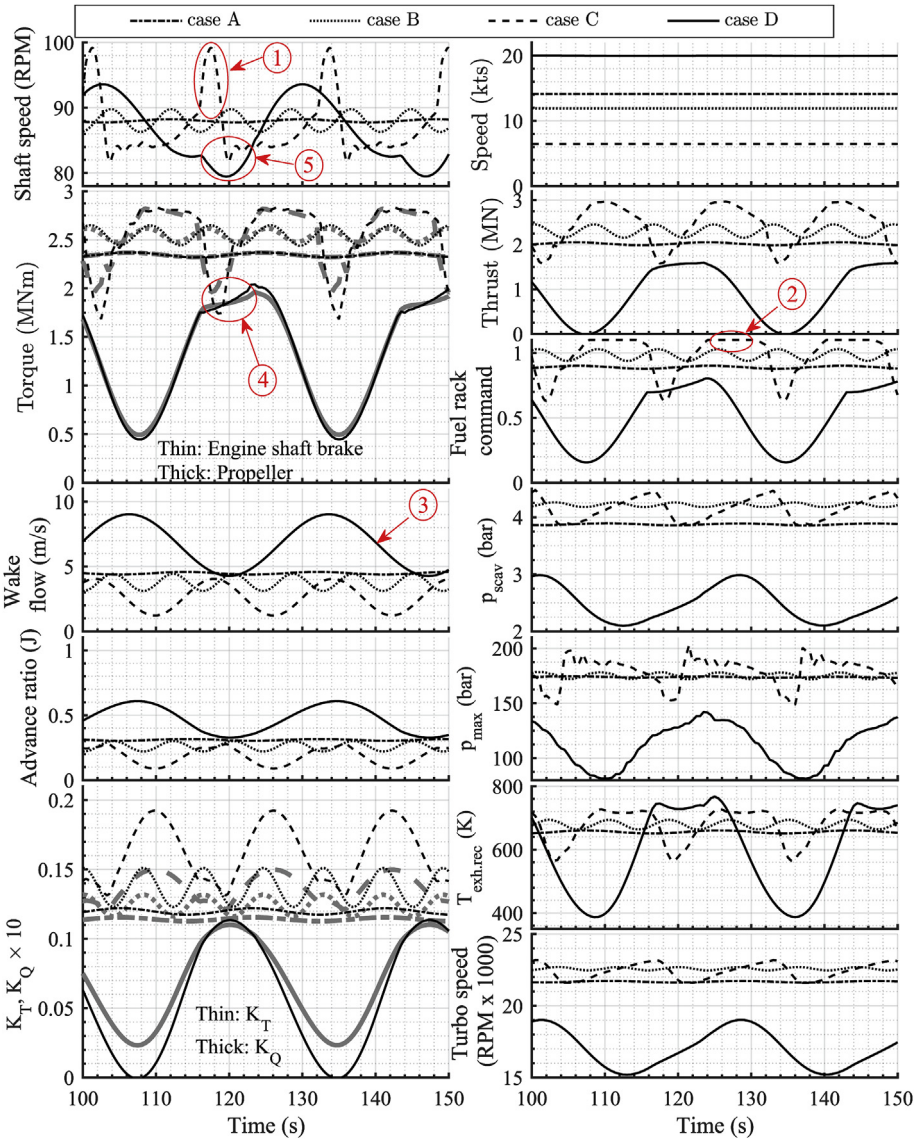

Fig. 21. The time series responses of the propulsion system in waves, low pass filtered at 2.5 Hz.

Table 5
Cases for discussion.

Case	H_{wave} (m)	λ_{wave} (m)	χ_{wave} (°)
A	3	512	90
B	3	192	180
C	5	512	180
D	5	192	0

unoptimized control of the valve close timing. Adding further constraints on the torque may help to mitigate the excessive pressure; however, it is not in the scope of this work.

For the compressor, the operation points are well within the surge line as shown in Fig. 23 except the case D, where the fluctuation of the system response was the greatest. This may require a better modeling of the air mass flow for the compressor model in this region.

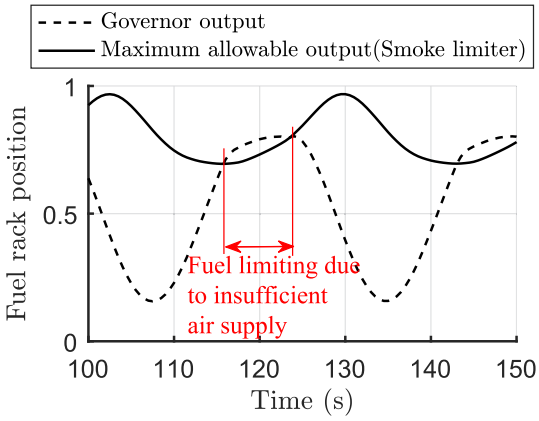

Fig. 22. Time series of fuel rack position command and the maximum allowable value from the smoke limiter.

Please cite this article in press as: Yum, K.K., et al., Simulation of a two-stroke diesel engine for propulsion in waves, International Journal of Naval Architecture and Ocean Engineering (2016), http://dx.doi.org/10.1016/j.ijnaoe.2016.08.004

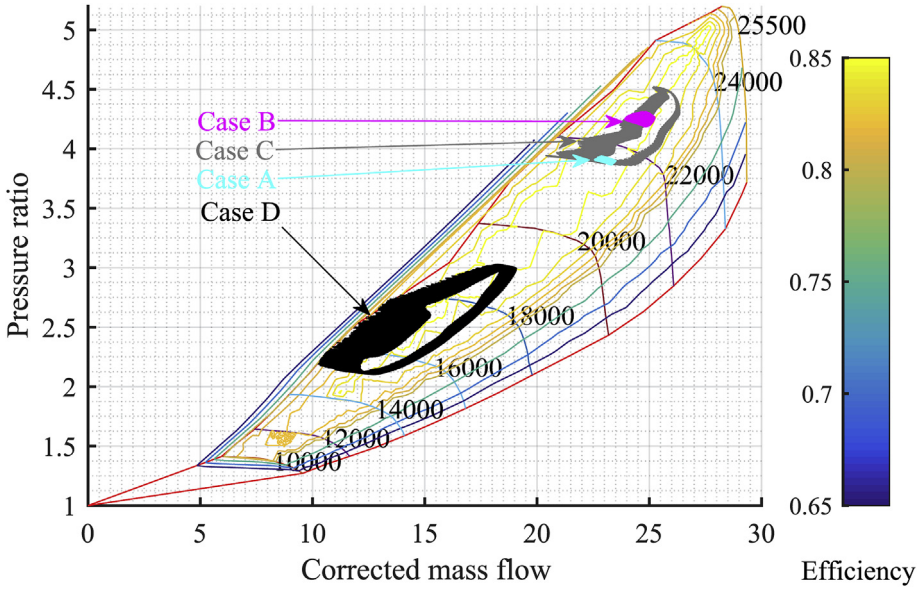

Fig. 23. Compressor operation of the main diesel engine.

As observed in the case C and D, an overall system response is the result of complex interactions between the external forces, the propeller inflow conditions, the vessel motions, the engine system dynamics and the control systems. As far as the propulsion system is concerned, it was shown that the diesel engine dynamics is often the reason for the slow response of the system. The nature of the feedback control system and turbocharger dynamics are main causes for such delays in our simulations. As shown in the sensitivity analysis for transient responses (Section 4.3), the mass moment of inertia of the propulsion system is not playing an important role. Therefore, in order to reduce the delay in the system response, one should enhance the engine response either by reducing the turbo-lag or by improving the control system. Adding an extra source of torque such as power-take-off and power-take-in could be an option to enhance the response, as demonstrated in the work of Yum et al. (2016).

5.2. System efficiency

With regard to the efficiency of the system, it can be broken down into the machinery efficiency and the propulsion efficiency. Also inn the transient operation, the average values of these efficiencies are used assess the performance of the system. They can be calculated as following.

$$\mathrm{BSFC} = \frac{3.6\cdot 10^9 \int \dot{m}_f dt}{\int M_{eng}\omega_{shaft} dt}$$
$$\eta_{prop} = \frac{\int (1-t)F_T \cdot \dot{x} dt}{\int M_{eng}\omega_{shaft} dt} \quad (31)$$

The average efficiency values of the machinery and the propulsion for different wave cases are shown in Fig. 24, where a polar plot is drawn for each wave length. A left side of a polar plot is showing BSFC for different wave directions (180° being head sea and 0° being following sea) and for different wave heights. We observe the BSFC values increasing, in other words, efficiency falling, as the vessel travels more toward to the incident wave and as the wave height increases. This is mainly because the engine is lower-load tuned, which means that the best efficiency is achieved at a relatively lower load, about 65%, see Fig. 18. Therefore, the increased engine load for adverse weather conditions results in higher BSFC. For the propulsion efficiency, the trend is similar and the efficiency drops as vessel travels toward the incoming waves and as the wave height becomes higher. For propellers, it largely depends on the vessel speed since the rotating speed is controlled at the same set point for all cases. Therefore, when the vessel speed drops in the adverse waves due to the increased resistance, the efficiency falls together. With regard to variations in wavelengths, we did not observe significant differences.

Finally, the influence of the transient load on BSFC is analyzed. First, the average transient BSFC is calculated according to (31) for all wave cases. In order to compare them with the steady state estimation, a BSFC map shown in Fig. 25 for the main engine was acquired by simulating various combinations of constant shaft speed set points and constant load torques. Then, the steady state estimate of BSFC was obtained by interpolating the BSFC with the speed-torque trace of each case as shown in Fig. 25 and calculating the average BSFC again using (31). The comparison of the transient BSFCs and steady state estimates is shown in Fig. 26. On each figure, a correlation coefficient between a wave condition and BSFC deviation is shown on the top.

Please cite this article in press as: Yum, K.K., et al., Simulation of a two-stroke diesel engine for propulsion in waves, International Journal of Naval Architecture and Ocean Engineering (2016), http://dx.doi.org/10.1016/j.ijnaoe.2016.08.004

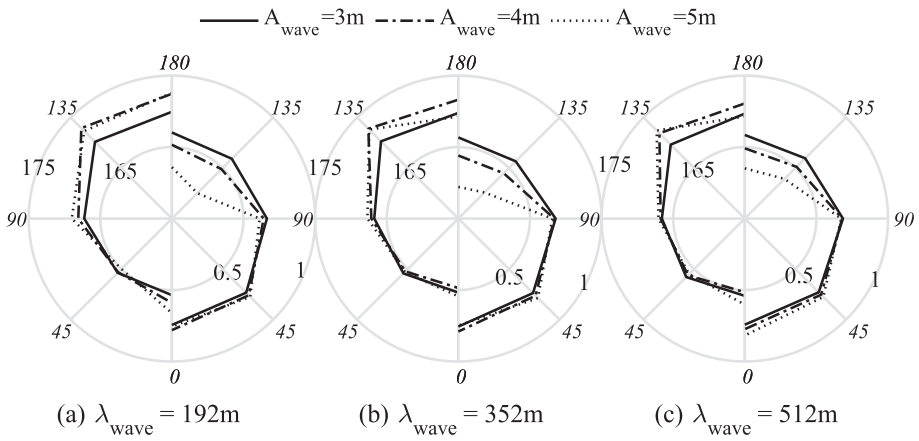

*Left hand side : BSFC(g/kWh)
Right hand side : Propulsion efficiency

Fig. 24. BSFC and propulsion efficiency comparison for different wave cases.

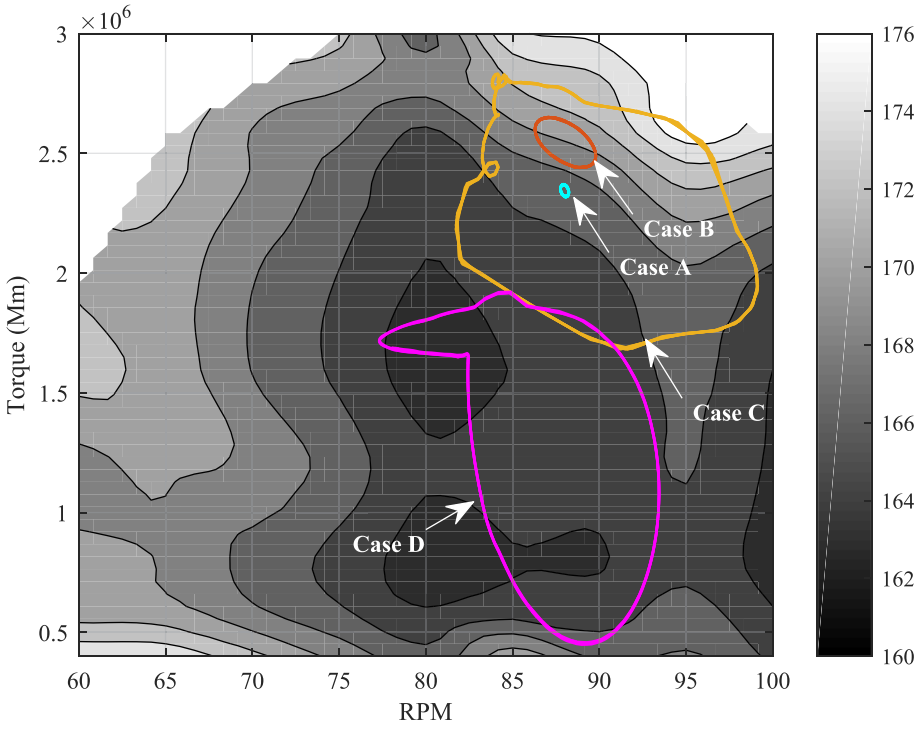

Fig. 25. Steady state BSFC map for the main engine and the system traveling path.

The difference is not significant except some cases of following sea (χ=0°). In the following sea cases, the mean engine load is significantly lower and the power variation amplitude is higher than other cases, which leads to higher degree of offset from the designed operation conditions. From the figure, it is found that the transient deviation is most related to the wave amplitude and the wave encounter angle. This suggests that the amplitude of the power variations plays an important role in the efficiency deviation due to transient loads. Since the engine system model is not validated against transient performance of the engine, especially with regard to BSFC, this result on the transient effect is only qualitatively valid.

6. Conclusion

In this paper, we have presented the simulation model for a mechanical propulsion system in waves involving the relevant parts: a vessel, a propeller, a main shaft, a diesel engine and controllers. The system model is inherently of multi-physical domains which followed a strictly defined framework for building it. Also the component models follow the physical principles of the actual processes as much as possible so that the model can be used for the transient simulations even the model is only validated against steady state measurements.

Please cite this article in press as: Yum, K.K., et al., Simulation of a two-stroke diesel engine for propulsion in waves, International Journal of Naval Architecture and Ocean Engineering (2016), http://dx.doi.org/10.1016/j.ijnaoe.2016.08.004

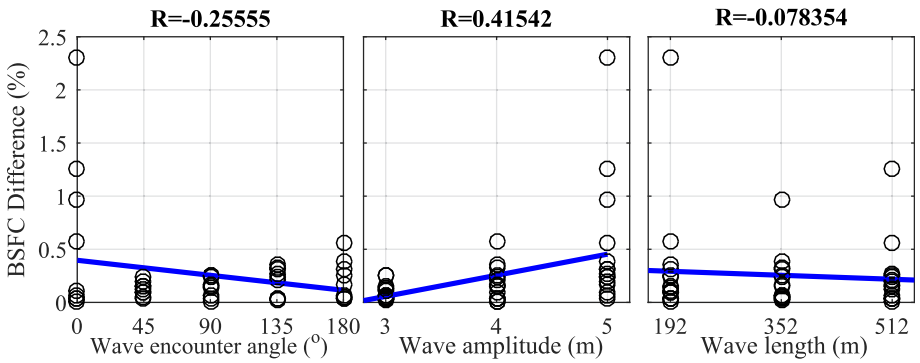

Fig. 26. BSFC comparison: Transient simulation vs. steady state estimate.

As observed in the simulation result, interaction between the environment, the physical components and the control system creates complex system responses. The numerical analysis of the system allows understanding of the complex physical process from a holistic point of view to local details. Finally it was also discovered that the transient effect on the efficiency of the diesel engine is not significant from the simulation result. It is difficult to generalize this finding because the transient performance of the simulation has not been quantitatively validated and the system response would differ from a case to another. Still, such a marine system simulator may allow the designers to assess the true capacity of the plant in various weather conditions and help them to achieve more optimized propulsion design.

Acknowledgments

This work is funded by the projects Design to Verification of Control Systems for Safe and Energy Efficient Vessels with Hybrid Power Plants (D2V, NFR: 210670/070), and Low Energy and Emission Design of Ships (LEEDS, NFR 216432/O70) where the Research Council of Norway is the main sponsor. This work is also supported by the Research Council of Norway through the Centers of Excellence funding scheme, project number 223254 AMOS.

Acronyms

BDC	bottom dead center
BSFC	break specific fuel consumption
CFD	computational fluid dynamics
CNO_x	concentration of NO_x emission
CPP	controllable pitch propeller
EEDI	Energy Efficiency Design Index
EVC	exhaust valve close
EVO	exhaust valve open
GHG	green house gas
IMO	International Maritime Organization
IPC	intake port close
IPO	intake port open
KPI	key performance indexes
LHV	lower heating value
RAO	response amplitude operator
ROHR	rate of heat release
RPM	revolution per minute.
SOC	start of combustion
SOI	start of injection
TDC	top dead center

Symbol

C_D	Discharge coefficient of an orifice
C_m	Mean piston speed
C_p	Specific heat capacity at constant pressure
D	Diameter
F	Fuel/air equivalence ratio
F_T	Thrust force of a propeller
M	Torque
R	Gas constant
T	Temperature
V	Volume
W	Work done to surroundings
Pr	Prandtl number
β_{scav}	Ratio of fresh air charge in the exhaust gas
$\dot{Q}$	Rate of heat transfer
γ	Heat capacity ratio
ω	Angular velocity
Re	Reynolds number
ρ	Density
τ	Time constant
φ	Crank angle
f_s	Stoichiometric fuel/air mass ratio
h	specific enthalpy
k	Heat transfer coefficient
m	Mass of gas unless stated otherwise.
m'	Added mass of a ship in the surge direction
m_f	Mass of the consumed fuel
p	Pressure
u	Specific internal energy

Subscript

A	Air
bf	Burned fuel
cv	Control volume

Please cite this article in press as: Yum, K.K., et al., Simulation of a two-stroke diesel engine for propulsion in waves, International Journal of Naval Architecture and Ocean Engineering (2016), http://dx.doi.org/10.1016/j.ijnaoe.2016.08.004

id ignition delay
ig ignition
inj injection

Appendix A. Calculation of the fuel/air equivalence ratio for the exhaust gas during a scavenging process

We assume that the fuel air equivalent ratio of the scavenging air entering the cylinder is zero, which means that it contains no burned mass of fuel. Therefore,

$$\dot{m}_{\text{in}} = \dot{m}_{\text{a,in}} \tag{A.1}$$

The mass flow rate of the exhaust gas through the valve, $\dot{m}_{\text{out}}$ consists of a part from the combustion gas and the other part from the fresh air charge in:

$$\dot{m}_{\text{out}} = \alpha\dot{m}_{\text{a,in}} + \dot{m}_{\text{bf,out}}\left(\frac{1+F_{\text{init}}\cdot f_{\text{s}}}{F_{\text{init}}\cdot f_{\text{s}}}\right) \tag{A.2}$$

where, F_{init} is the fuel/air equivalence ratio before IPO and α is a positive factor that is less than 1 and $\dot{m}_{\text{bf,out}}$ is the mass flow of burned fuel through at the exhaust valve from the combustion gas. Then, the fuel/air equivalence ratio of the exhaust gas at the valve outlet can be expressed as below:

$$F_{\text{out}} = \frac{\dot{m}_{\text{bf,out}}}{f_s\dot{m}_{\text{a,out}}} = \frac{\dot{m}_{\text{bf,out}}}{f_s\left(\alpha\dot{m}_{\text{a,in}} + \frac{\dot{m}_{\text{bf,out}}}{F_{\text{init}}f_s}\right)} \tag{A.3}$$

where $\dot{m}_{\text{a,out}}$ is mass flow of the unburned air at the exhaust valve.

The mass fraction of fresh charge air content (β) in the combustion gas at the exhaust valve can be expressed as following:

$$\beta = \frac{\alpha\dot{m}_{\text{a,in}}}{\alpha\dot{m}_{\text{a,in}} + \dot{m}_{\text{bf,out}}\left(\frac{1+F_{\text{init}}\cdot f_{\text{s}}}{F_{\text{init}}\cdot f_{\text{s}}}\right)} \tag{A.4}$$

The equation (A.4) can be solved for $\alpha\dot{m}_{\text{a,in}}$,

$$\alpha\dot{m}_{\text{a,in}} = \frac{\beta}{1-\beta}\dot{m}_{\text{bf,out}}\left(\frac{1+F_{\text{init}}f_{\text{s}}}{F_{\text{init}}f_{\text{s}}}\right) \tag{A.5}$$

Inserting (A.5) in (A.2) and solving for $\dot{m}_{\text{bf,out}}$, we obtain,

$$\dot{m}_{\text{bf,out}} = (1-\beta)\frac{F_{\text{init}}f_{\text{s}}}{1+F_{\text{init}}f}\dot{m}_{\text{out}} \tag{A.6}$$

Finally, inserting (A.5) and (A.6) in (A.3), we can express F_{out} as a function of *beta* and F_{init} as following:

$$F_{\text{out}} = \frac{(1-\beta)F_{\text{init}}}{\beta F_{\text{init}}f_s + 1} \tag{A.7}$$

References

Albrecht, A., Grondin, O., Le Berr, F., Le Solliec, G., 2007. Towards a stronger simulation support for engine control design: a methodological point of view. Oil Gas Sci. Technol. Rev. IFP 62 (4), 437–456. http://dx.doi.org/10.2516/ogst:2007039.

Annand, Walter John Dinnie, Roe, Geoffrey Ernest, 1974. Gas Flow in the Internal Combustion Engine: Power, Performance, Emission Control, and Silencing. GT Foulis.

Benson, R.S., Pool, D.E., may 1965. The compressible flow discharge coefficients for a two-dimensional slit. Int. J. Mech. Sci. 7 (5), 337–353. http://dx.doi.org/10.1016/0020-7403(65)90063-9. ISSN 00207403. http://www.sciencedirect.com/science/article/pii/0020740365900639.

Bergman, Theodore L., Incropera, Frank P., DeWitt, David P., Lavine, Adrienne S., 2007. Fundamentals of heat and mass transfer. In: Dekker Mechanical Engineering, vol. 6. John Wiley & Sons, ISBN 9780471457282. http://dx.doi.org/10.1016/j.applthermaleng.2011.03.022. http://www.osti.gov/energycitations/product.biblio.jsp?osti_id=6008324.

Campora, U., Figari, M., 2005. Numerical simulation of ship propulsion transients and full-scale validation. Proc. Inst. Mech. Eng. Part M J. Eng. Marit. Environ. 217 (1), 41–52. http://dx.doi.org/10.1243/147509003321623130. ISSN 1475-0902.

Churchill, S.W., Bernstein, M., may 1977. A correlating equation for forced convection from gases and liquids to a circular cylinder in crossflow. J. Heat Transf. 99 (2), 300–306. http://dx.doi.org/10.1115/1.3450685. ISSN 0022-1481.

el Moctar, Ould, Lantermann, Udo, Mucha, Philipp, Höpken, Jens, Schellin, Thomas E., aug 2014. RANS-based simulated ship maneuvering accounting for hull-propulsor-engine interaction. Ship Technol. Res. 61 (3), 142–161. http://dx.doi.org/10.1179/str.2014.61.3.003. ISSN 0937-7255. http://www.tandfonline.com/doi/abs/10.1179/str.2014.61.3.003.

Faltinsen, O.M., Minsaas, K.J., Liapis, N., Skjørdal, S.O., 1980. Prediction of resistance and propulsion of a ship in a seaway. In: 13th Symposium on Naval Hydrodynamics. The Shipbuilding Research Association of Japan, Tokyo, Japan.

Finol, C.A., Robinson, K., 2006. Thermal modelling of modern engines: a review of empirical correlations to estimate the in-cylinder heat transfer coefficient. Proc. Inst. Mech. Eng. Part D J. Automob. Eng. 220 (12), 1765–1781. http://dx.doi.org/10.1243/09544070jauto202. http://pid.sagepub.com/content/220/12/1765.abstract.

Ghojel, J.I., aug 2010. Review of the development and applications of the Wiebe function: a tribute to the contribution of Ivan Wiebe to engine research. Int. J. Engine Res. 11 (4), 297–312. http://dx.doi.org/10.1243/14680874JER06510. ISSN 1468-0874. http://jer.sagepub.com/content/11/4/297.short.

Hepperle, Martin, 2007. JavaFoil. http://www.mh-aerotools.de/airfoils/javafoil.htm.

Heywood, J.B., 1988. Internal Combustion Engine Fundamentals. McGraw Hill.

Karnopp, Dean, 1979. State variables and pseudo bond graphs for compressible thermofluid systems. In: National Conference Publication – Institution of Engineers, Australia, pp. 861–865. http://www.scopus.com/inward/record.url?eid=2-s2.0-0018680832&partnerID=40&md5=50fdb71a5e858a73457b5f4a1880ad9b.

Kyrtatos, N.P., Theodossopoulos, P., Theotokatos, G., Xiros, N.I., 1999. Simulation of the overall ship propulsion plant for performance prediction and control. In: MarPower99 Conference, (JANUARY 1999).

Loukakis, T.A., Sclavounos, P.D., 1978. Some extensions of the classical approach to strip theory of ship motions, including the calculation of mean added forces and moments. J. Ship Res. 22 (1).

Minsaas, K., Faltinsen, O., Persson, B., 1983. On the importance of added resistance, propeller immersion and propeller ventilation for large ships in a seaway. In: Second International Symposium on Practical Design in Shipbuilding (PRADS), pp. 149–159. Seoul and Tokyo.

Papanikolaou, A., Zaraphonitis, G., Tech, Nat, Shigunov, V., El Moctar, O., 2014. Energy efficient Safe ship operation (Shopera). Influ. EEDI Ship Des. 1 (2012), 24–25.

Pedersen, Eilif, Engja, Hallvard, 2000. A bond graph model library for modelling diesel engine transient performance. In: ISME Tokyo 2000, vol. 2, pp. 447–455. Tokyo.

Rakopoulos, Constantine D., Giakoumis, E.G., 2006. Review of thermodynamic diesel engine simulations under transient operating conditions. SAE Paper (2006-01):884.

Sher, E., 1990. Scavenging the two-stroke engine. Prog. Energy Combust. Sci. 16 (2), 95–124.

Taskar, Bhushan, Koosup Yum, Kevin, Steen, Sverre, Pedersen, Eilif, 2016. The effect of waves on engine-propeller dynamics and propulsion performance of ships. Ocean Eng. 122, 262–277. http://dx.doi.org/10.1016/j.oceaneng.2016.06.034. http://dx.doi.org/10.1016/j.oceaneng.2016.06.034.

Winterthur Gas & Diesel, 2015. General Technical Data. https://www.wingd.com/en/media/general-technical-data/.

Wu, Ping-Chen, 2013. A CFD Study on Added Resistance, Motions and Phase Averaged Wake Fields of Full Form Ship Model in Head Waves. Osaka University. Doctoral dissertation. http://ir.library.osaka-u.ac.jp/dspace/handle/11094/26191.

Yang, Jianguo, Wang, Qinpeng, 2013. Hardware-in-Loop simulation technology of high-pressure common-rail electronic control system for low-speed marine diesel engine. In: Bari, Saiful (Ed.), Diesel Engine – Combustion, Emissions and Condition Monitoring, Chapter 10. InTech, ISBN 978-953-51-1120-7, p. 278. http://www.intechopen.com/books/diesel-engine-combustion-emissions-and-condition-monitoring.

Yum, K.K., Pedersen, E., 2016. Architecture of Model Libraries for Modeling Internal Combustion Engines. Mathematical and Computer Modelling of Dydnamical Systems (Submitted for review).

Yum, Kevin Koosup, Tasker, Bhushan, Skjong, Stian, Pedersen, Eilif, Steen, Sverre, 2016. Simulation of a Hybrid marine propulsion system in waves. In: Proceedings of 28th CIMAC World Congress, Number 202. CIMAC, Helsinki.

Zacharias, F., 1967. Analytical representation of the thermodynamic properties of combustion gases. SAE Technical Paper, 670930. http://dx.doi.org/10.4271/670930.

Please cite this article in press as: Yum, K.K., et al., Simulation of a two-stroke diesel engine for propulsion in waves, International Journal of Naval Architecture and Ocean Engineering (2016), http://dx.doi.org/10.1016/j.ijnaoe.2016.08.004